


8-2017

STRUCTURAL AND FUNCTIONAL EFFECT OF PHOSPHORYLATION ON AMPA RECEPTORS

Caitlin E. Nurik

Follow this and additional works at: https://digitalcommons.library.tmc.edu/utgsbs_dissertations

 Part of the [Biochemistry, Biophysics, and Structural Biology Commons](#), and the [Medicine and Health Sciences Commons](#)

Recommended Citation

Nurik, Caitlin E., "STRUCTURAL AND FUNCTIONAL EFFECT OF PHOSPHORYLATION ON AMPA RECEPTORS" (2017). *The University of Texas MD Anderson Cancer Center UTHealth Graduate School of Biomedical Sciences Dissertations and Theses (Open Access)*. 793.
https://digitalcommons.library.tmc.edu/utgsbs_dissertations/793

This Dissertation (PhD) is brought to you for free and open access by the The University of Texas MD Anderson Cancer Center UTHealth Graduate School of Biomedical Sciences at DigitalCommons@TMC. It has been accepted for inclusion in The University of Texas MD Anderson Cancer Center UTHealth Graduate School of Biomedical Sciences Dissertations and Theses (Open Access) by an authorized administrator of DigitalCommons@TMC. For more information, please contact digitalcommons@library.tmc.edu.

STRUCTURAL AND FUNCTIONAL EFFECT OF PHOSPHORYLATION ON AMPA RECEPTORS

by

Caitlin Edmunds Nurik, B.A.

APPROVED:

Vasanthi Jayaraman, PhD

Advisory Professor

Darren Boehning, PhD

Jeffrey Frost, PhD

Shane Cunha, PhD

John Spudich, PhD

APPROVED:

Dean, The University of Texas

MD Anderson Cancer Center UTHealth Graduate School of Biomedical Sciences

STRUCTURAL AND FUNCTIONAL EFFECT OF PHOSPHORYLATION ON
AMPA RECEPTORS

A

DISSERTATION

Presented to the Faculty of

The University of Texas

MD Anderson Cancer Center UTHealth

Graduate School of Biomedical Sciences

in Partial Fulfillment

of the Requirements

for the Degree of

DOCTOR OF PHILOSOPHY

by

Caitlin Edmunds Nurik, B.A.

Houston, Texas

August, 2017

Dedication

This thesis is dedicated to my family and friends, who have seen me through every challenge during and prior to the last four years of my education.

Acknowledgements

I would first and foremost like to acknowledge my advisor and mentor, Dr. Vasanthi Jayaraman. Her tireless effort on behalf of her students is truly an inspiration, and her compassion is limitless. I also wish to thank my labmates, Dr. Drew Dolino and Dr. Sana Shaikh, for their help on my project and countless offerings of wisdom. To Doug Litwin, M.S., my brilliant labmate and friend, I offer my thanks for making the lab an enjoyable and comfortable place to work. To Dr. David Maclean, I thank you for your extraordinary wisdom and your generosity in sharing it with me. To Drs. Rita Sirrieh and Swarna Ramaswamy, I thank you for all of the training and wonderful company you offered me.

To my collaborators, I thank you all for your wonderful training and research, particularly Dr. Darren Boehning.

Lastly, I must acknowledge my family, without whom I would never have been able to accomplish what I have, including but certainly not limited to an advanced degree in the sciences. To my wonderful husband, words cannot express how much your support the last many years has helped and comforted me. To my loving parents, your support has been invaluable to this process, in addition to the entire rest of my life as well. To my siblings, I thank you for your love and support.

STRUCTURAL AND FUNCTIONAL EFFECT OF PHOSPHORYLATION ON AMPA RECEPTORS

Caitlin Edmunds Nurik, B.A.

Advisory Professor: Vasanthi Jayaraman, Ph. D.

The α -amino-3-hydroxy-5-methyl-4-isoxazolepropionic acid (AMPA) receptor is the primary contributor to neuronal fast excitatory transmission, and plays a key role in learning and memory. Previous studies have established that residues S818, S831, and T840 in the C-terminal segment of GluA1 homomeric AMPA receptor are phosphorylated by PKC, and phosphorylation at these sites leads to an increase in receptor conductance. We show that the domain inclusive of those sites alters its secondary structure due to phosphorylation (using glutamate substitution as a mimic) in a lipid charge dependent manner using Fourier transform infrared spectroscopy. We also indicate a strong shift in the domain's conformational landscape using single molecule FRET. Using wild-type GluA1 receptors, as well as glutamate and alanine to mimic phosphorylation and dephosphorylation respectively, we show based on FRET measurements that the C-terminal segment moves away from the membrane upon phosphorylation. Additionally, the FRET between the C-terminal segment and inner leaflet of the plasma membrane increases upon activation of the receptor for the triple alanine dephosphorylated receptor indicating a further motion towards the membrane associated with activation of the receptor. The phosphomimetic receptor, on the other hand, shows no change in FRET associated with activation of the receptor. However, addition of the lipid sphingosine restores this change in FRET due to activation for the phosphomimetic receptor. Using single channel current recordings we confirm that there is an increase in all conductance

levels of the AMPA receptor in the phosphomimetic receptor and show that this increase in conductance is reversed by incorporation of sphingosine in the membrane or addition of poly-L-lysine. Thus using FRET and functional measurements we show that the plasma membrane lipid content is critical in mediating the phosphorylation mediated functional changes in GluA1 AMPA receptor.

Table of Contents

<u>Approval.....</u>	<u>i</u>
Title page	ii
Dedication	iii
Acknowledgements	iv
Abstract	v
Table of Contents.....	vii
List of Illustrations	x
Abbreviations	xi
CHAPTER 1: INTRODUCTION TO AMPA RECEPTORS	1
Synaptic transmission and Balance of Ion Channels.....	1
An Introduction to Ionotropic Glutamate Receptors	2
Architecture of the AMPA Receptor.....	3
Significance of AMPA GluA1 C-terminal Domain to Receptor Function.....	5
Auxiliary subunits and its role.	6
CHAPTER 2 : GENERAL METHODS AND THEORY	8
Vibrational Spectroscopy.....	8
Fluorescence Resonance Energy Transfer.....	13
Overview	13
Whole Cell FRET Acquisition.....	15

<i>Single Molecule FRET Acquisition</i>	17
<i>Assessment of FRET Techniques</i>	19
CHAPTER 3: STRUCTURAL STUDIES OF AMPA GLUA1 C-TERMINAL SEGMENT	21
<i>Introduction</i>	21
<i>Methods Specific to this Chapter</i>	24
<i>Peptide Sample Preparation for Fourier Transform Infrared & Single Molecule FRET</i>	24
<i>Lipid Vesicle Preparation</i>	25
<i>Fourier transform infrared spectroscopy measurements</i>	25
<i>Single Molecule Measurements & Analysis</i>	26
<i>smFRET Data Analysis</i>	27
<i>Results</i>	27
<i>Vibrational Spectroscopy Examining the AMPA GluA1 C-terminal Segment</i>	27
<i>Single-molecule FRET Studies of the AMPA GluA1 C-terminal Segment</i>	30
<i>Discussion</i>	32
CHAPTER 4 CONFORMATIONAL AND FUNCTIONAL CHANGES IN THE FULL LENGTH RECEPTOR	33
<i>Introduction</i>	33
<i>Methods Specific to this Chapter</i>	33
<i>Mutagenesis & Construct Selection</i>	33
<i>Cell culture and Transfection for Spectrometry and Imaging</i>	34

<i>Spectrometry & FRET Imaging.....</i>	35
<i>Cell culture and transfection for electrophysiology.....</i>	36
<i>Patch-clamp recording.....</i>	36
<i>Analysis of unitary AMPA-receptor currents.....</i>	37
<i>Results.....</i>	39
<i>Changes in FRET between the GluA1 C-terminal segment and the plasma membrane.....</i>	39
<i>Effect of local membrane charge on the position of the GluA1 C-terminal segment .</i>	48
<i>Imaging based FRET measurements.....</i>	49
<i>The effect of PKC phosphorylation and lipid composition on GluA1 function at the single-channel conductance.....</i>	52
<i>Discussion.....</i>	59
<i>DISCUSSION - FINAL THOUGHTS & FUTURE DIRECTIONS.....</i>	64
<i>Future Directions.....</i>	64
<i>Final Thoughts.....</i>	64
<i>Works Cited</i>	65
<i>Vita.....</i>	81

List of Illustrations

<i>Figure 1. Crystal Structure of the AMPA Receptor.....</i>	<i>4</i>
<i>Figure 2. Interferometry in FTIR.....</i>	<i>9</i>
<i>Figure 3. FTIR is Applied to Assessment of Secondary Protein Structure.....</i>	<i>12</i>
<i>Figure 4. Spectral Overlap in FRET Fluorophore Pairs.....</i>	<i>14</i>
<i>Figure 5. Composition Analysis of GluA1 CTD.....</i>	<i>23</i>
<i>Figure 6. FTIR Spectra of AMPA GluA1 CTD.....</i>	<i>28</i>
<i>Figure 7. Single Molecule FRET in the GluA1 CTD.....</i>	<i>31</i>
<i>Figure 8. FRET Showing GluA1 Proximity to Inner Leaflet.....</i>	<i>40</i>
<i>Figure 9. Movement of the GluA1 CD toward the Plasma Membrane Upon Channel Opening.....</i>	<i>42</i>
<i>Figure 10. Lack of Change in Fluorescent Cells Expressing Donor only and Acceptor only</i>	<i>44</i>
<i>Figure 11. Lower FRET between GluA1 CTD and Lyn-GFP at the Plasma Membrane upon Phosphorylation</i>	<i>46</i>
<i>Figure 12. Phosphorylation Eliminates Activation-Induced Changes in FRET and is Restored by Positive Lipid.....</i>	<i>47</i>
<i>Figure 13. Single Cell Imaging Verifies FRET Change due to Phosphorylation.....</i>	<i>50</i>
<i>Figure 14. AMPA Receptor Unitary Conductance Influenced by Interactions with Inner Leaflet of Plasma Membrane.....</i>	<i>53</i>
<i>Figure 15. Screening C-terminal Membrane Interactions Prevents Phosphorylation- Induced Increase in Unitary Current.....</i>	<i>56</i>

Abbreviations

ANOVA	Analysis of Variance
AMPA	α -amino-3-hydroxy-5-methyl-4-isoxazolepropionic acid
ATD	Amino terminal domain
CaMKII	Calmodulin-dependent Protein Kinase II
CTD	Carboxy-terminal domain
C-terminal	Carboxy-terminal
FRET	Fluorescence Resonance Energy Transfer
FTIR	Fourier Transform Infrared Spectroscopy
GABA_A	γ -aminobutyric acid receptor
iGluR	Ionotropic glutamate receptor
GFP	Green fluorescent protein
LBD	Ligand binding domain
NMDA	N-methyl-D-aspartate
PKA	Protein kinase A
PK	Poly-L-lysine
PKC	Protein kinase C
PR	Proximity Ratio
RFP	Red fluorescent protein
R.M.S.	Root Mean Square

CHAPTER 1: INTRODUCTION TO AMPA RECEPTORS

Synaptic transmission and Balance of Ion Channels

Synaptic transmission is the process by which neurons communicate with one another. This occurs through the targeted vesicular release (pre-synaptic) of signaling molecules known as neurotransmitters, which bind to receptors on the receiving neuron (post-synaptic). The receptors, activated by the neurotransmitter, then carry out the signaling process. This signal can be inhibitory or excitatory according to the purpose of the cell-to-cell communication. For instance, the activation of anion-specific GABA_A receptors is the most common mechanism for inhibitory signaling in the mammalian central nervous system, and it functions by coordinating with glutamatergic cellular activity (1-3). It acts to repolarize the cell membrane, halting potential excitation of the cell by cation specific ionotropic glutamate receptors. Neuronal health depends upon the balance of these complex signaling pathways, and thus extensive research in the fields of biophysics and cellular and molecular biology has been dedicated to the understanding of the function and modulation of these receptors. My project focuses on the excitatory proteins - ionotropic glutamate receptors.

An Introduction to Ionotropic Glutamate Receptors

The primary mediators of excitatory neurotransmission in the central nervous system are the ionotropic glutamate receptors. Ubiquitously expressed and activated physiologically by glutamate, ionotropic glutamate receptors are cation selective ion channels thus leading to an influx of predominantly sodium ions under resting conditions resulting in depolarization of the neuron. In the continued presence of glutamate the receptors eventually desensitize leading to the closure of the transmembrane channel.

Ionotropic glutamate receptors (iGluRs) being the primary mediators of excitatory neurotransmission in the mammalian central nervous system, their function is critical to synaptic strength that underlie learning and memory (4-9). There are three subtypes of iGluR's – NMDA, AMPA, and Kainate receptors. They are categorized as NMDA and non-NMDA. Although all three subtypes are activated by the same neurotransmitter (in NMDA's case both glutamate and glycine must bind), they are delineated most acutely by their different gating kinetics. The α -amino-3-hydroxy-5-methyl-4-isoxazolepropionic acid receptor (AMPA receptor) is primarily responsible for the fast portion excitatory neurotransmission, on the millisecond timescale (10-12). This begins the depolarization required for NMDA to more slowly release a channel-blocking Mg^{2+} and activate to allow calcium ion flux, leading to further depolarization and signal propagation (13-15). Another key quality differentiating not just iGluRs but even subtype specific iGluRs is ion specificity. NMDA receptors are calcium

permeable(15). AMPA receptor are primarily Na^+ permeable; however, RNA editing in a transmembrane loop yields Ca^{2+} permeability (16, 17).

Architecture of the AMPA Receptor

AMPA receptors are composed of homomeric or heteromeric combinations of 4 subunits GluA1-4, which convey unique trafficking and gating properties to the receptors. iGluRs are modular in structure, comprising four domains bound together by flexible linkers (18) (Figure 1). Extracellularly, there is the amino terminal domain, as well as the more membrane-proximal ligand-binding domain, to which agonists like glutamate bind and induce channel opening. These are arranged as dimers of dimers (18) . The transmembrane domain serves as the actual cation-channel pore while the carboxyl terminus serves as the primary target for posttranslational modifications including phosphorylation and palmitoylation (19-24). iGluR's have been extensively characterized by x-ray crystallography as well as Cryo-electron microscopy. Most structural studies in the field have explored the extracellular domains and their roles in mediating channel gating and desensitization. Detailed crystal structures for all three iGluR subtypes have been used to correlate structural changes to their functional consequences in the pursuit of potential therapeutic development (25-27).

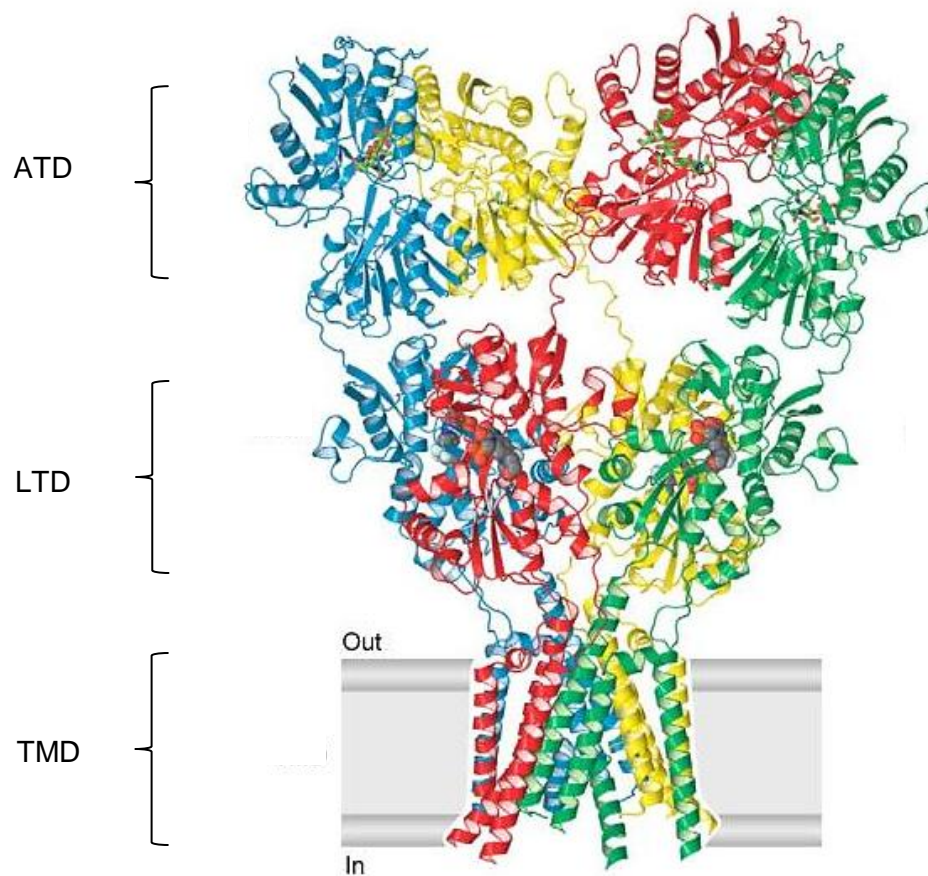


Figure 1. Crystal Structure of the AMPA Receptor.

The AMPA receptor is modular in nature, comprising four domains. The amino terminal domain (ATD) and ligand binding domain (LBD) are extracellular, while the transmembrane domain occupies the plasma membrane. The intracellular carboxy-terminal domain has been crystallized. PDB ID: 3KG2 Used with permission. (18) (Sobolevsky, A. I., M. P. Rosconi, and E. Gouaux. 2009. X-ray structure, symmetry and mechanism of an AMPA-subtype glutamate receptor. Nature 462: 745-756.)

Significance of AMPA GluA1 C-terminal Domain to Receptor Function

The AMPA receptor GluA1 carboxy terminus, comprising residues 809-889 of the receptor, is the least characterized of the four modular domains due to the lack of crystallographic or electron microscopic data on the domain. Its protein-protein interactions as well as known posttranslational modifications modulate channel trafficking, stabilize the receptor synaptic sites via cytoskeletal interactions, and affect receptor insertion into the membrane; of particular interest is the role of phosphorylation in this segment (21, 28-40).

Phosphorylation by protein kinase A at S845 in GluA1 is necessary for trafficking to the synapse but negatively affects channel function (19, 29). In the intracellular loops that link together the transmembrane domains, CaMKII phosphorylation in the first intracellular loop of the domain (intracellular) at S567, is necessary for receptor targeting to the synapse (41). PKC phosphorylation has a number of effects on the receptor and on the channel. One of its four phosphorylation sites binds to protein 4.1N which in turn binds actin to stabilize the channel at the membrane (38, 40). Most relevant to my studies, PKC phosphorylation at C-Terminal residues S818, S831, and T840 in the GluA1 AMPA receptor subunit results in increases in the conductance of the receptor by about 25% (28, 29, 42). GluA1 phosphorylation has been shown to be critical for the strengthening of synapses known as long term potentiation (39).

These three sites and their effects on the receptor are the primary focus of this dissertation project. The goal is to determine the mechanism of action employed by these three modifications to affect the channel function. Their ability

to affect the channel without changing the receptor's function drastically could present a unique opportunity to modulate the channel population by tweaking activity, rather than using a strong agonist or antagonist. The uniqueness of these three sites to the GluA1 subunit amongst AMPA receptor subunits also presents the potential for subunit specific modulation. GluA1 subunit loss is indicated in anxiety(43) and its overexpression is indicated in stress-enhanced fear learning, a mouse model of post-traumatic stress disorder(44). GluA1 is also overexpressed in the addictive response to cocaine and morphine in mouse models, so a drug that could reduce function in these overexpressed pathologies could potentially ameliorate drug-seeking behavior (45). Perhaps most importantly, GluA1 expression and phosphorylation are altered greatly in mouse models of Parkinsonism (46). Given the role of GluA1 and phosphorylation in disease models understanding the structure-function modulation due to phosphorylation becomes critical.

Auxiliary subunits and its role.

iGluRs, including GluA1-containing AMPA receptors, are endogenously co-expressed with a number of modulating proteins called transmembrane AMPA Receptor regulatory proteins (TARPs) that help direct trafficking and enhance function (increased conductance compared to receptors expressed alone) (47, 48). The most well-characterized TARP is TARP $\gamma 2$, which is widely expressed in multiple brain regions including the hypothalamus (49). Our studies use TARP $\gamma 2$ to aid expression and trafficking of GluA1 homomers, and to offer physiological relevance to our data given that it is a membrane protein.

Since both TARP $\gamma 2$ and phosphorylation increase channel function, it is key to determine phosphorylation mediated changes in the presence of TARP $\gamma 2$. Functional changes due to phosphorylation have been shown to persist in the presence of TARP $\gamma 2$ through noise analysis of electrophysiological data on GluA1 homomers (28, 50). Here we have extended these studies to gain a more comprehensive understanding by performing single channel current recordings that provide detailed insight into changes in the conductance levels associated with different substates and additionally spectroscopic studies are also obtained to provide insight into conformational changes.

CHAPTER 2 : GENERAL METHODS AND THEORY

Vibrational Spectroscopy

Fourier Transform Infrared Spectroscopy (FTIR) is a light-based technique in which the absorption/emission spectrum of a sample is obtained to facilitate analysis of secondary structure in protein samples (51-54).

The principle of the method is based on sample exposure to a broad beam of light (comprising a spectrum of wavelengths). This light is processed through an interferometer, which selectively exposes the sample to different wavelengths via a system of mirrors within the instrument, one of which is controlled mechanically to move toward or away from the beamsplitter (Figure 2). The modulated light source is accompanied by a laser, whose frequency is used to as a “clock” which triggers sampling.

The raw data produced, known as an interferogram, is then processed by performance of a Fourier transform, yielding a spectrum. The raw data itself is by definition a plot in which the independent variable is the degree to which the moveable mirror has been displaced and the resultant dependent variable as intensity received at the detector. This process can be described mathematically. The signal an interferogram receives at its detector, $I(x)$, is:

$$I(x) = B(\nu)\cos 2\pi\nu x$$

Equation 1.

where x is the displacement of the moveable mirror from its maximal possible distance and $B(\nu)$ is the intensity of the light source, presented as a function of its frequency ν .

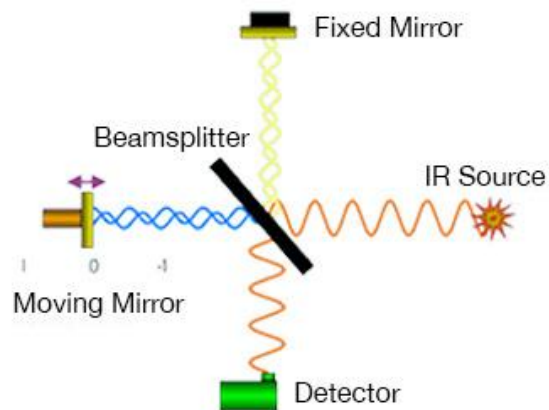


Figure 2. Interferometry in FTIR

. A set of multiple mirrors, including one that moves, is used to vary the wavelength of light being exposed over time, to assess the ability of a sample to absorb the light at different wavelengths. (ThermoFisher)

Equation 1 is actually a simplification of the related equation which applies more aptly to FTIR, in which a range of frequencies is probed. In this case, the interferogram's intensity can be described by:

$$I(x) = \frac{1}{2\pi} \int_{-\infty}^{\infty} B(\nu) \cos 2\pi \nu x d\nu$$

Equation 2.

in which the range of ν values is accounted for. This equation allows one to relate the interferogram to the spectrum. Obviously, no instrument has an infinite range of frequencies available, so in practice a truncation is made based on the frequency limitations of a given source.

FTIR data is generally presented as an absorption spectrum, and as such can be converted via the following equation based on intensity measurements:

$$A(\nu) = -\log_{10} \tau(\nu) = -\log_{10} I/I_o = a(\nu)lc$$

Equation 3.

in which $A(\nu)$ is the absorbance, $\tau(\nu)$ is the transmittance of the sample, l is path length, c is concentration of the sample, and the I/I_o is the ratio of light intensity radiated to that received by the detector. Spectra can be background subtracted using air or nitrogen and buffer-only controls to reveal a final spectrum representing only the sample of interest.

Previous studies have established distinct wavelengths (or wavenumbers in cm^{-1}) at which known secondary structure makeup in a sample is to be expected (54, 55). This allows for ensemble studies to assess the overall secondary structure makeup of a protein sample in multiple conditions (ie ligand-

bound versus Apo in a receptor or over the course of denaturation) (56-60). An example of the use of FTIR for assessing secondary structural changes due to protein phosphorylation is shown in Figure 3.

FTIR harbors the advantage of fairly high signal-to-noise ratio as well as that of being a fairly time-efficient technique, since the interferometer exposes samples to a broad range of wavelengths quickly (61). Many samples and controls can be measured in one day, even if, as in my studies, each sample is repeated and averaged. Limitations to FTIR include that it is, like ensemble FRET, only a measure of a population and is not applicable to single molecule or single cell studies. Nevertheless, it offers an accessible way to assess overall protein secondary structure. In our case, it allowed us to determine that a protein domain largely dismissed as intrinsically disordered does indeed have secondary structure elements, and that they are affected by modification (phosphorylation) as well lipid charge environment.

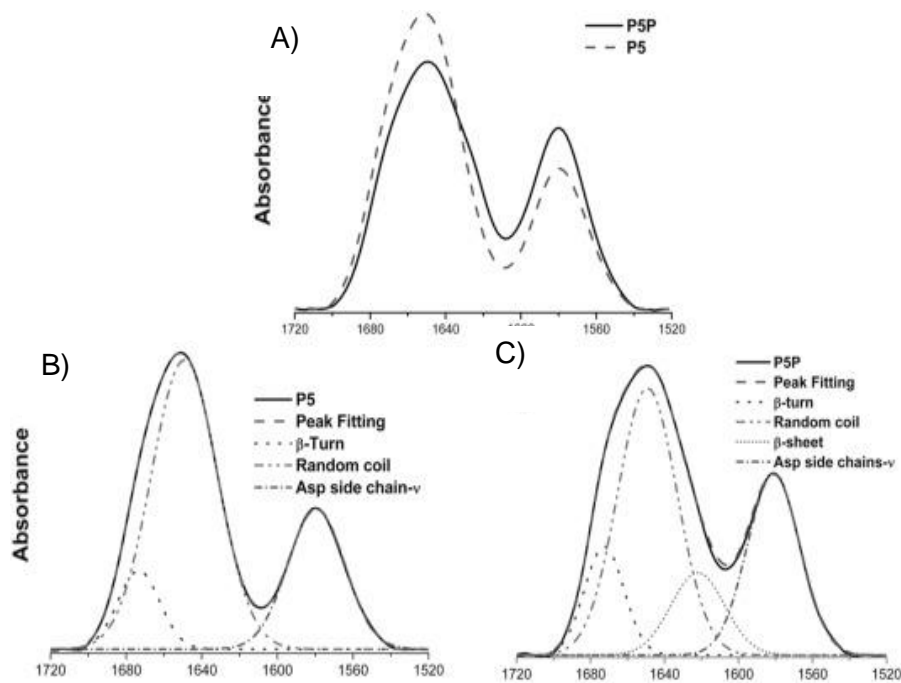


Figure 3. FTIR is Applied to Assessment of Secondary Protein Structure.

FTIR here is applied to assess the different absorbance spectra of a dentin phosphoprotein P5 with and without phosphorylation. Initial spectra A) are analyzed for secondary structure and corresponding curve analysis for each is shown B) for the unphosphorylated and C) phosphorylated phosphoprotein. Used with permission (62). (Villarreal-Ramirez, E., D. Eliezer, R. Garduño-Juarez, A. Gericke, J. M. Perez-Aguilar, and A. Boskey. 2017. Phosphorylation regulates the secondary structure and function of dentin phosphoprotein peptides. *Bone* 95: 65-75.)

Fluorescence Resonance Energy Transfer

Overview

Fluorescence resonance energy transfer is the passing of energy non-radiatively from a donor fluorophore to an acceptor fluorophore. This technique is widely referred to as a molecular ruler because it allows distance and distance changes to be measured in fluorescently labeled samples (63, 64). This technique depends upon the overlap, defined as an integral function, J , of the donor emission and acceptor excitation spectra in order for transfer to occur. Figure 4 explains this further. The overlap integral can be mathematically described by this equation:

$$J (M^{-1}cm^{-1}nm^{-1}) = \frac{\int \varepsilon(\lambda)f(\lambda)\lambda^4d\lambda}{\int f(\lambda)d\lambda}$$

Equation 4.

where ε is the extinction coefficient, $f(\lambda)$ is the emission spectrum, λ is the wavelength.

FRET is a technique that often is accompanied by structural data such as crystallography or Cryo-electron microscopy in order to aid in the selection of the fluorophore labeling sites in protein/s of interest, gauge their proximity, and select fluorophores accordingly. The overall range of the technique is approximately 10-100 Å and can be used to measure the change in distance between fluorophores within that range (63, 64).

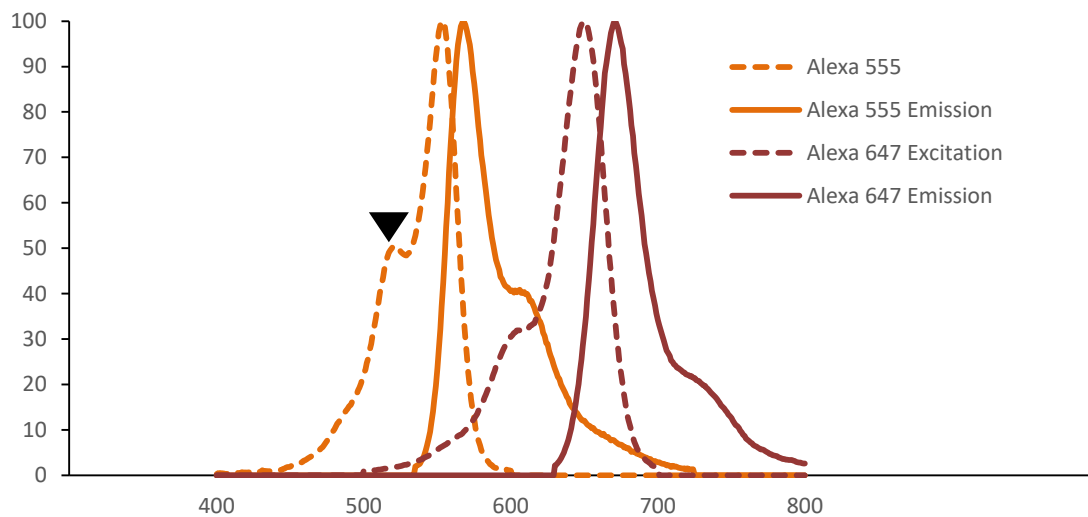


Figure 4. Spectral Overlap in FRET Fluorophore Pairs

FRET pairs must have overlapping emission and excitation spectra. In order to measure the efficiency of the non-radiative transfer, rather than direct emission of the acceptor fluorophore, excitation wavelength must be selected to excite only the donor directly (black arrow). The interval of overlap between the donor emission (orange solid) and the acceptor excitation spectra (red dotted) is integral to the interaction and affects the value of the pair's R_0 (R_0 will be described further below).

This transfer's efficiency is detected and then used to assess the distance between fluorophores. This calculation uses the Förster equation, below:

$$E_T = \frac{R_0^6}{R^6 + R_0^6}$$

Equation 5.

where the distance R between fluorophores can be calculated based upon the efficiency of the energy transfer E_T and R_0 the distance at which the fluorophores have half-maximal energy transfer efficiency. Many common commercial fluorophores have published R_0 values, but they can also be calculated by this equation with empirical knowledge of the refractive index of the experimental medium:

$$R_0 = \left(\frac{8.79 \times 10^5 \times \kappa^2 \times \phi_D \times J}{n^4} \right)^{1/6}$$

Equation 6.

where J is the overlap integral of the donor and acceptor emission and excitation spectra respectively, ϕ_D is the donor quantum yield, κ^2 is the orientation factor (assumed to be $\frac{2}{3}$), and n is the refractive index of the solution medium being used. Selection of fluorophores must take their R_0 and any expected distance between labeling sites of the sample into account.

Whole Cell FRET Acquisition

FRET has many applications as a technique, from whole cell expression to single molecule acquisition. Whole cell studies can quantify FRET using the

rate of decay of the donor fluorophore to measure energy transfer efficiency by the following equation:

$$E = \frac{k_{FRET}}{k_{FRET} + \sum k_{other}}$$

Equation 7.

where k_{FRET} represents only the rate of decay due only of energy transfer, and

$k_{FRET} + \sum k_{other}$ represent additive total decay rate for the donor fluorophore.

This decay equation can be converted to fluorophore lifetimes by converting each rate to its inverse:

$$E = \frac{\tau_D - \tau_{DA}}{\tau_D}$$

Equation 8.

where the lifetimes of the donor while transferring energy τ_{DA} and that of the donor-only τ_{DA} are used to determine efficiency of transfer. This process can also be performed by measuring sensitized acceptor emission – emission by the acceptor during FRET- to assess transfer efficiency. This technique is an adapted form of FRET called luminescent resonance energy transfer (LRET) which uses lanthanide dyes like terbium chelate, as donors. The lifetime of the organic dyes like tetramethyl-rhodamine used as acceptors are orders of magnitude shorter than the donors, and therefore can be treated as the donor lifetime (65, 66). Commonly used in our lab, this technique carries the advantage of avoiding the measurement of donor fluorophores that do not have an associated acceptor molecule due to uneven labeling or loss of active acceptor molecules to photobleaching (65).

For my studies that expressed AMPA receptors in cells, a genetically encoded labeling approach was used in order to allow for complete labeling of two intracellular protein domains. GFP- and RFP-tagged proteins were used. In these experiments, FRET is less a molecular ruler and rather a gauge of relative shifts between fluorophores. Protein/s can be over-expressed and measured in a cuvette using a spectrometer. Then, comparisons can be between controls a) expressing the donor-only to gauge how much the donor could fluoresce with no acceptor absorbing its energy, and b) expressing the acceptor only to gauge potential bleed-through (direct excitation of the acceptor leading to fluorescence). This technique was also applied to single cell FRET measurements using fluorescent microscopy to narrow acquired data to the plasma membranes of individual cells. The basal and condition-induced shift (in my case, activation of the receptor by glutamate) can be measured over time by the scope, in the case of basal FRET, and by simple division to determine fold change in FRET upon condition change.

Single Molecule FRET Acquisition

For my studies, single molecule FRET on fluorescently labeled peptides was performed to assess changes in conformational preference due to protein modification by phosphorylation. This method is intensity based, and acquires both donor and acceptor intensity measurements for single molecules over time.

These intensity measurements can be integrated over that time, then used to calculate the relative proximity ratio, E_{PR} ,

$$E_{PR} = \frac{I_A}{I_D + I_A}$$

Equation 9.

where I_A and I_D are the integrated intensities of the acceptor and donor fluorophores(67).

Although E_{PR} is an indicator of molecular shifts, it is not a precise measurement of FRET because it fails to account for differences in the fluorophores' quantum yields and the differences in their detection efficiency by the scope. Thus, a correction factor, γ , can be applied such that:

$$\gamma = \frac{\Delta I_A}{\Delta I_B}$$

Equation 10.

Thus, the correction factor can be applied to the relative proximity ratio to normalize it:

$$E_{corr} = \frac{I_{A,corr}}{I_{D,corr} + I_{A,corr}} = \left(\frac{I_A}{I_D + I_A} \right) \gamma$$

Equation 11.

where $I_{A,corr}$ and $I_{D,corr}$ are the corrected integrated intensities for the acceptor and donor fluorophores, and E_{corr} is the resultant calculated efficiency of energy transfer.

There are multiple types of single molecule FRET instruments which can be divided into those which use immobilized samples and those whose samples are diffusing freely through a small volume. Each type has advantages and disadvantages. Diffuse samples do not struggle with potential reduced mobility of the protein of interest (68, 69). However, that freedom comes at the cost of losing the wash steps taken for an immobilized sample to aid in purification and especially removal of any free fluorophores that remain unattached to protein but in solution. This means that purification is of the utmost importance for diffuse samples. All acquisitions for this dissertation project were acquired using immobilized samples which used a biotin-streptavidin linkage to bind peptides to slides. Although protein purification is not a major concern, the slides and each reagent required to treat them serve as a potential source of contamination, which must be prevented for reliable data acquisition.

Assessment of FRET Techniques

Each FRET-based technique has different benefits to offer its users. Whole cell FRET techniques do not require extensive protein purification, which can disrupt protein stability if too harsh. Moving to single cell acquisition in whole cells offers localization of the acquisition to a targeted area, which can help reduce unwanted acquisition of internalized protein during ensemble spectrometric studies of surface-expressed proteins. Single molecule FRET is unique in that it offers the opportunity to examine a range of conformational diversity in a given molecule rather than an ensemble of protein. However, it

comes at the cost of needing a purified sample. In the case of synthetic peptides, purification was not of great concern for my single molecule acquisitions.

CHAPTER 3: STRUCTURAL STUDIES OF AMPA GLUA1 C-TERMINAL SEGMENT

Introduction

The goal of the project is to determine the mechanism of PKC phosphorylation on AMPA GluA1 receptor function. To form a hypothesis regarding the mechanism, and given the dearth of structural information available, we first needed to obtain some structural information about the domain.

The cytoplasmic domain of GluA1, comprising residues 809-889, has been largely dismissed as intrinsically disordered. It is a fair assessment that a degree of disorder is present in the domain because a looser conformation could logically allow conformational changes to facilitate protein-protein binding events. Multiple proteins which bind to the domain are key to the channel's trafficking and function including as SAP97 and m-LIN-10, which participate in receptor localization, and 4.1 which facilitates a stabilizing cytoskeletal interaction (40, 70-72). The challenges this domain has presented in crystallization also defend a disordered structure but could be equally explained by the existence of multiple, stable conformational states.

Recent studies as well as the data to be presented in this chapter suggest that at least local levels of structure exist in the domain. A previous study which analyzed a small part of the C-terminal segment, a peptide composed of amino acids 828-849, via solution-state NMR suggested that long-range conformational shifts may occur due to S831 phosphorylation and suggested potential helical

content based of molecular modeling (28). Residue composition analysis using Composition Profiler also suggested that the amino acid makeup of the domain does not match that of a classically disordered protein library (Figure 5) (73).

Here, I have used vibrational and single molecule FRET based spectroscopic measurements to study the overall secondary structure and conformational landscape of the domain. Structural studies were specifically focused upon the domain region containing the three sites of interest (S818, S831, and T840); peptides comprising residues 809-842 were used for the following studies presented in this chapter.

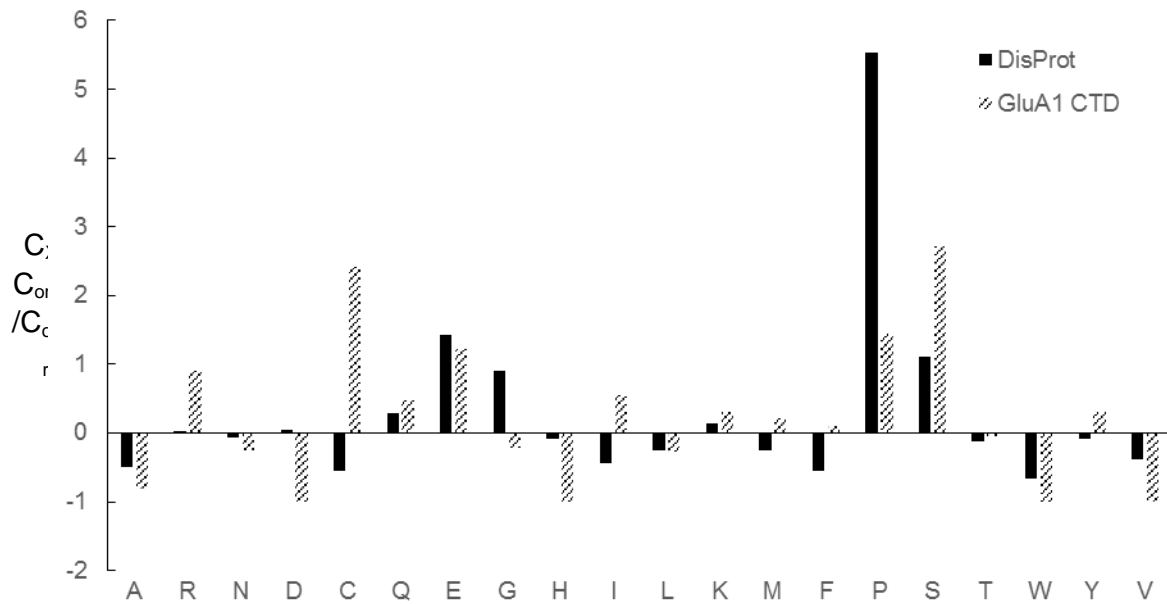


Figure 5. Composition Analysis of GluA1 CTD

Composition Profiler analysis comparing the GluA1 carboxy-terminal domain's percent residue composition to that of canonical libraries of disorder (DisProt, charted in pattern). Percentage residue content C_x for both are compared to percentage residue content C_{order} of a canonical ordered library available through Composition Profiler with permission of (74) and plotted. Negative values indicate that the sample contains more of a given residue than the ordered library and vice versa.

Methods Specific to this Chapter

Peptide Sample Preparation for Fourier Transform Infrared & Single Molecule

FRET

Peptides were synthesized by Peptide 2.0 and NeoBio Labs and their purity was verified by HPLC. Peptides represents the first half of the domain with the sequences for unphosphorylated protein as

efcyksrseskrmkgfSlipqqSineairtStlC and for the phosphomimetic protein as efcyksrseEkrmkgfSlipqqEineairtSElC. Capitalized residues are modifications to the wild type sequence including glutamate phosphomimic sites S818E, S831E, and T840E, as well as a central C->S mutation to allow for maleimide cysteine labeling at only desired sites bookending the phosphorylation sites).

Phosphomimetic proteins were selected to ensure that degree of “phosphorylation” remained constant between experiments and due to previous characterization confirming the functional replication of PKC phosphorylation by glutamate substitution in the domain (29, 75). Peptides were ordered with an amino-terminal biotin tag to facilitate single molecule studies. Samples were dissolved and aliquoted for storage at -20°C. For single molecule FRET studies, samples were diluted to 2 uM for labeling in 1X PBS (137 mM NaCl, 2.7 mM KCl, 10mM Na₂HPO₄, 1.8 mM KH₂PO₄, PH=7.4). FTIR samples were run at 6 mg/mL in 1X PBS in D₂O to prevent water contamination. For single molecule studies, fluorescent labeling with donor Alexa555 and acceptor Alexa647 maleimide dyes was performed in buffer at a 1:1:3 mole ratio of peptide:donor:acceptor. Samples were rotated 1 hour prior to dilution for single molecule acquisition. Free dyes

were cleared from the sample once it was loaded and bound to slides by sequential washes.

Lipid Vesicle Preparation.

Because GluA1 is a membrane protein, lipids were present in all of the structural studies. All lipids for vesicle preparation were purchased from Avanti. Neutral lipid was 1-palmitoyl-2-oleoyl-sn-glycero-3-phosphocholine (POPC) 18:1/16:0 and charged were 1-palmitoyl-2-oleoyl-sn-glycero-3-phospho-L-serine (POPS) 18:1/16:0. All lipids were purchased as sodium salts. Lipid stocks were prepared at 20 mg/ml total, in 1X PBS (137 mM NaCl, 2.7 mM KCl, 10mM Na₂HPO₄, 1.8 mM KH₂PO₄). Stocks were aqueous for single molecule and fluorescence studies. Stocks for FTIR studies were made in 1X PBS in D₂O-based buffer.

Fourier transform infrared spectroscopy measurements.

A Nicolet Nexus 870 spectrometer was used to collect FTIR spectra. Spectra were obtained using an adjustable path length infrared cell holder (Aldrich). The protocol for acquisition was adapted from those previously used in our lab (76-78) and used to obtain the FTIR spectra of phosphomimetic and unphosphorylated GluA1 C-terminal peptides. Because spectra in the infrared region of 1600-1700 cm⁻¹ exhibit a large absorption of water at ≈1600 cm⁻¹, all FTIR studies were conducted in D₂O based buffer system and prepared immediately before acquisition to reduce contamination from ambient humidity. Samples were loaded by injection into a sealed liquid transmission cell, and a path length of 50 μm was used. Spectra were collected at 4 cm⁻¹ resolution and

held at a constant temperature of 15°C. Spectral peaks arising from buffer/lipid content were subtracted using a background buffer spectrum of each sample. Data analysis and collection were performed using Omnic (ThermoFisher Scientific) and Origin 8.6/9.0 software (OriginLab). Data was normalized to allow visualization of changes between samples.

Single Molecule Measurements & Analysis.

All single molecule measurements were acquired using protocols developed previously by the Landes lab and in collaboration with the Jayaraman lab (27, 79). Clean slides were passivated using polyethylene glycol solution to reduce nonspecific binding and dried under nitrogen. Labeled sample peptides prepared as noted above were flowed into the chamber and allowed to bind through via a biotin streptavidin linkage. Unbound fluorophores were removed by sequential wash with buffer (1X PBS) and sealed in a solution of lipid vesicles with oxygen scavenging solution to preserve fluorophore stability. The prepared sample chamber was secured to the P-517.3CL Physik Instrumente closed-loop-x-y-z-piezo stage, which allows for precise movement of the slide and sample to enable focusing at high resolution (80, 81). The laser was used to excite single molecules at a time using a power density of 50 watts/cm². Emitted light collected and subsequently passed through a Chroma Technology zet532nm notch filter toward the detector box. It was then passed through a 640-nm high-pass dichroic mirror (Chroma 640 DCXR) and collected with two corresponding avalanche photodiode detectors (SPCM AQR-15, Perkin Elmer). The filters used were set to 570 (donor) and 670 (acceptor) nm by band-pass filters (NHPF-

532.0, Kaiser Optical and ET585, Chroma Technology) in accordance with the emission peaks of the fluorophores. Molecules were selected within 10 x 10 μm raster-scanned areas at a time. The laser was focused on them and donor and acceptor channels recorded until photobleaching occurred, generally 5-15 seconds.

smFRET Data Analysis.

Emission intensity trajectories were recorded at 1ms-resolution, then binned into 10-ms frames to improve signal-to noise ratios (27). In-house MATLAB script was used to analyze and denoise by wavelet decomposition, as described previously (26, 82, 83).

Results

Vibrational Spectroscopy Examining the AMPA GluA1 C-terminal Segment

In order to examine secondary structure in the GluA1 CTD, we collected the vibrational spectra of the unphosphorylated and phosphomimetic proteins (Figure 6). These experiments show a difference in secondary structures of their GluA1 carboxy-terminal domains (Figure 6).

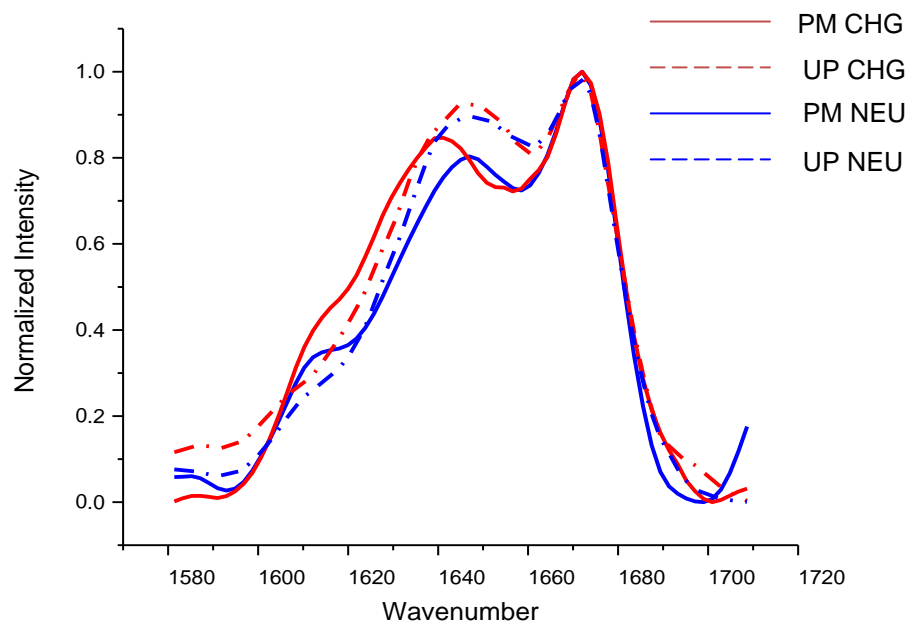


Figure 6. FTIR Spectra of AMPA GluA1 CTD

FTIR spectra of the unphosphorylated (UP, dashed) and phosphomimetic (PM, solid) peptides of the GluA1 C terminus show varied levels of secondary structure. Peptide samples were run in the presence of small unilamellar vesicles of net neutral (blue, NEU) and charged lipids (red, CHG) for unphosphorylated and phosphomimetic peptides.

The unphosphorylated protein exceeds the phosphoprotein in helical content regardless of lipid charge, as shown by the higher 1620 -1650 cm^{-1} peaks (dotted traces). However, in the phosphomimetic peptide (solid traces), this shift in alpha helix was accompanied by an increase at the 1620 cm^{-1} peak, indicative of increased beta-sheet in the protein. Most importantly, the phosphoprotein shows an additional increase beta-sheet in the charged lipid environment (red solid trace). Horizontal misalignment of the peaks is most likely due to altered solvation between the peptides (84).

Firstly, and most fundamentally, these data confirm that this domain is not completely disordered but rather possesses multiple secondary structure elements. The molecular model predicting both a helix and a large degree of random coil in the domain is in agreement with the peaks at 1620-1650 cm^{-1} and 1670 cm^{-1} in both phosphorylation states in both lipid conditions (29, 85). Interestingly all four conditions tested showed nearly identical peaks for coil, suggesting that the ultimate charge environment yielded by phosphorylation state and lipid environment did not affect the degree of disorder in the protein but rather mediated the proportions of alpha helix to beta sheet. These data also align with the previous study in which NMR spectroscopy upon a small segment of the domain suggested long range conformational shifts due S831 phosphorylation (29). These data indicate that the mechanism by which PKC phosphorylation affects the GluA1 channel could include a conformational shift in the protein, and that this conformational change is regulated in part by the surrounding lipid charge environment.

Single-molecule FRET Studies of the AMPA GluA1 C-terminal Segment

In conjunction with our vibrational spectroscopy, we performed single molecule FRET experiments to examine the conformational landscape of the GluA1 carboxy-terminal domain. (Figure 7). We found that phosphorylation profoundly affected the structure and resultant dynamic range in the domain via smFRET.

The phosphomimetic proteins exhibited a narrower range of efficiencies and as well a stronger preference for one efficiency state near $E=0.4$ in both net-neutral and charged lipid environments compared with the unphosphorylated. These data support the conclusions of the vibrational data, indicating a shift in conformational preference accompanying the secondary structure shift observed by FTIR.

The effects of lipid charge on the domain's conformational preference are not as conclusive; this is potentially due to the limitation of the technique that individual peaks in data may represent more than one conformation in three-dimensional space. However, charged lipid proximity did appear to increase the overall FRET efficiency probed by the phosphomimetic domain, with an opposite overall effect on the unphosphorylated protein as compared to net-neutral surroundings.

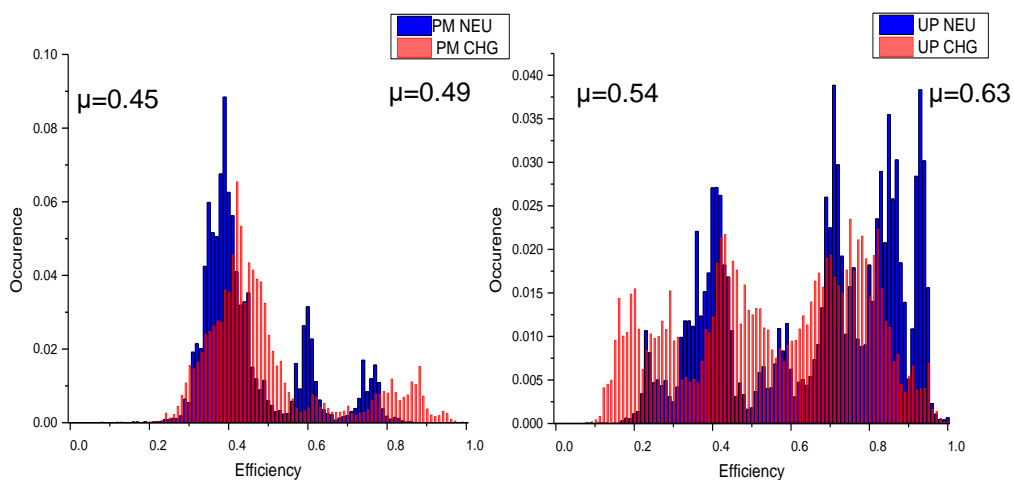


Figure 7. Single Molecule FRET in the GluA1 CTD

Single molecule studies in neutral (NEU, blue) and charged (CHG, red) lipid environments show reduced dynamics due to phosphomimicry. The phosphomimetic peptide (PM, left) showed a narrower range of FRET efficiency than the unphosphorylated protein (UP, right). Denoised data represent N=43 (UP NEU), N=32 (PM NEU), N= 49 (UP CHG), N=43 (PM CHG) molecules. Weighted average FRET efficiency μ is shown for each sample.

Discussion

To investigate the mechanism of PKC phosphorylation on the function of the AMPA GluA1 receptor, we have examined the structure and conformation of the AMPA GluA1 subunit carboxy-terminal domain. We took the vibrational spectrum of the domain in the unphosphorylated state and mimicked phosphorylation with glutamate substitutions in presence of net neutral and charged lipids. All conditions showed clear secondary structure elements indicating that the domain contains local levels of order. Phosphorylation reduced helical content in the domain and increased beta sheet content; this increase was more pronounced in the presence of charged lipids indicating lipid regulation in PKC's mechanism of action on the channel. To examine the conformational shifts that accompany the secondary structure changes due to phosphorylation, we performed single molecule FRET upon the domain. Phosphorylation clearly narrows the range of conformations probed by the protein, causing a strong preference for one peak surrounding $E=0.4$. The shifts in both the unphosphorylated and modified proteins in the charged lipid compared with the net neutral surroundings may account for the shifts in helical and sheet content observed in the FTIR investigation. Together, these data support the hypothesis that PKC phosphorylation causes a physical shift of the domain, altering and limiting its conformation. The independent effect of lipid charge on the domain indicates that this shift may constitute a motion with regard to the plasma membrane; thus we next moved on to verify this mechanism in functional receptors.

CHAPTER 4 CONFORMATIONAL AND FUNCTIONAL CHANGES IN THE FULL LENGTH RECEPTOR

Introduction

There is great precedent for the use of fluorescence-based structural and dynamics investigations, and functional characterization, in the AMPA receptor and other iGluRs. However, these studies have been largely applied to the outer three domains, where there is evidence of structural stability, replicable conformational shifts, and well-characterized patterns of gating/kinetics.

With evidence of secondary structure content and conformational shifts in the intracellular segment of GluA1 due to phosphorylation (Chapter 3), we set about to apply functional and fluorescence-based techniques to the understudied carboxy-terminal domain. Fluorescence studies are a useful tool for measuring conformational shifts, and as such were an ideal application for investigating motion of the C-terminal domain relative to the negatively charged plasma membrane. Upon identifying an activation-induced motion of the domain, which is disrupted by phosphorylation, we correlated our hypothesis to actual channel function using single-channel electrophysiology.

Methods Specific to this Chapter

Mutagenesis & Construct Selection

Triple glutamate (GluA1P) and triple alanine (GluA1AAA) mutants were made by sequential point mutation in the GluA1 wild type gene in a pcDNA3.1(+) vector at S818, S831, and T840. For whole cell FRET studies, fluorescent clones GluA1P-RFP and GluA1AAA-RFP, as well as wild type GluA1-RFP, were made

by fast cloning and sequential mutation and sequencing verified (Genewiz). Expression was confirmed via Western blot and for RFP clones also confirmed visually by appearance of RFP in cell samples. Lyn-GFP was selected as the donor fluorophore due to its direct trafficking to cell inner leaflet, and was kindly sent by Dr. Takanari Inoue and expression and localization verified by visual inspection of transfected cells (86).

Cell culture and Transfection for Spectrometry and Imaging

HEK293T cells were maintained in DMEM with 10% fetal bovine serum and antibiotics. Cells were transfected with GluA1P-RFP or GluA1AAA-RFP mutants with TARP $\gamma 2$ to aid in trafficking and expression and with Lyn GFP as donor at a ratio of 4:1:0.25 for spectroscopy and 1:1:.04 or 1:2:.04 for imaging using jetPRIME transfection reagent (Polyplus), and media changed after 4-6 hours. Transfections were maintained under 100 μ M NBQX to inhibit channel activation prior to experimentation. For imaging, cells were imaged 48 hours post-transfection. For spectroscopy, transfected cells were harvested after 48-72 hours and washed three times with extracellular buffer (145 mM NaCl, 1.8 mM $MgCl_2$, 1 mM $CaCl_2$, 3 mM KCl, 10 mM glucose, and 10 mM HEPES, pH 7.4).

For experiments with altered lipid environment, 100 μ M sphingosine (Avanti) was added into the culture medium 4 hours prior to harvesting the cells at 37°C. Sphingosine (Avanti) solution was prepared by repeated sonication in extracellular buffer before addition into culture medium (86).

Spectrometry & FRET Imaging

Spectroscopic acquisition was performed with a QuantaMaster model QM3-SS (Photon Technology International) spectrometer. GFP and RFP excitation wavelengths used were 420 nm and 520 nm, respectively. Emission spectra for Apo were collected with real-time background correction enabled with step size 5 nm, and 1 s integration time using Felix32 software over the range 440-700 nm. After Apo acquisition, cells were activated with 1 mM glutamate and 100 μ M cyclothiazide to prevent desensitization. Data analysis was completed in Origin Pro. Spectra were measured in triplicate, and all transfections were repeated at least three times. HEK cells with no transfection (control for scatter) and donor-only samples were acquired as background controls. Significance of changes in spectra due to activation and due to phosphorylation was evaluated by repeated measure *t*-tests and independent two-tailed *t* tests, respectively, significance was defined at $P < 0.05$.

Single cell imaging acquisition used a Nikon Eclipse Ti confocal microscope and MetaFluor version 7.8.3.0 to acquire the FRET signal. FRET protocols were written in-house (Darren Boehning lab, McGovern Medical School at UTHealth) and were optimized based on the level of receptor expression to maximize image quality. Regions of interest were selected only at the plasma membranes. Logged imaging data were analyzed using Origin Pro. Basal FRET and fold change upon activation with 1 mM glutamate and 100 for each sample was averaged (data points are plotted with averages for clarity). For single cell Apo samples, N= 15, 16, 20, and 15 cells for GluA1AAA, Glu1AAA+sphingosine,

GluA1P, and GluA1P+sphingosine, respectively. For each activation induced single cell sample, N=5 cells per group, and the significance of change between cells expressing GluA1AAA and GluA1P groups was assessed using independent two-tailed *t* tests. Significance of changes due to activation was assessed by repeated measure *t* test, as in the ensemble measurements.

Cell culture and transfection for electrophysiology

For the patch-clamp experiments, HEK 293T cells were cultured in DMEM with 10% fetal bovine serum and antibiotics. Cells seeded on poly-L-lysine coated glass coverslips were transiently transfected with 1 µg of total cDNA GluA1P or GluA1AAA per coverslip X-tremeGENE 9 DNA transfection reagent (Roche) according to the manufacturer instructions. Wild-type GluA1 or GluA1P and TARP γ2 cDNAs were co-transfected at ratios of 1:1 to 1:2. The enhanced green fluorescent protein (eGFP, 0.2 µg) was included in all the transfections to aid in identifying transfected cells.

Patch-clamp recording

Single channel recordings from outside-out patches excised from transfected cells were performed 24-72 hours after transfection. All recordings were done at room temperature with an EPC-9 patch clamp amplifier (HEKA) and PatchMaster (HEKA) acquisition software. The recordings were made at a holding potential of -100 mV. Patches were held in external solution (150 mM NaCl, 3mM KCl, 2mM CaCl₂, 1 MgCl₂, and 10 HEPES (pH adjusted to 7.4 with NaOH). Patch pipettes with open tip resistance 4-10 MΩ were filled with internal

solution (135 mM CsF, 33 mM CsOH, 2 MgCl₂, 1 CaCl₂, 11 EGTA and 10 HEPES, pH 7.4.

A theta glass pipette mounted on a piezoelectric bimorph was used to deliver external solution with and without 10 mM glutamate to excised outside-out patches (87). The rate of solution exchange as measured from open tip responses was 200-400 μ s. The bath was superfused constantly with external solution at a rate of 1-2 ml/min. Low-pass filtered voltage pulses were applied across the piezoelectric bimorph with protocols controlled by the PatchMaster acquisition software. Patches were screened for peak inward currents ≤ 25 pA in response to 100 ms applications of 10 mM glutamate to avoid recording large numbers of receptors. Unitary currents were recorded during the continuous application of glutamate. The proportion of closed time in all the records was high (0.82 ± 0.02 , N = 20 patches) and did not differ significantly for the different data sets. No patches contained evidence of double openings during continuous application of glutamate.

For experiments with reduced charge along the inner leaflet, poly-L-lysine (10 μ g/ml) was added into the internal pipette solution. In some experiments transfected cells were incubated with 100 μ M sphingosine as in the whole cell studies.

Analysis of unitary AMPA-receptor currents

Single-channel currents recorded during continuous application of 10 mM glutamate were analog low-pass filtered sequentially by two 4-pole Bessel filters in the EPC-9 (cut-off frequencies 10 kHz and 3 kHz), sampled at 20 kHz, and

written directly to the hard drive of the computer in segments of 250 ms. Individual segments were inspected and the holding (baseline) current (1 to 7 pA) was set to zero. Recordings inspected for obvious artifacts and stable baseline currents before being analyzed with QuB (88). Individual data segments were concatenated in QuB and the resulting data file was subjected to digital Gaussian low-pass filtering at 2 kHz, resulting in closed-channel r.m.s noise values of 200-400 fA. Drift or transient shifts in the closed-channel current were manually corrected.

The time resolution was set at 5 sample intervals 250 μ s, and the data file was then idealized with QuB analysis software to identify single-channel transitions and estimate conductance levels and open channel durations (89). The kinetic model used for the idealization contained two closed states and one open state for each of the four open levels present in AMPA receptor records (90). All states were connected to each other, allowing in principle all types of transitions between the five different conductance levels. The resultant idealization was superposed on the data and inspected to verify that it accurately represented the results and edited to remove spurious events.

Shut times and open durations for each of the four open levels and log-likelihood fitting of the relevant distributions were determined in QuB (91, 92). The records contained many brief open events, which were excluded at a threshold of 300 or 400 μ s. Final analysis was performed with IGOR Pro (Wavemetrics). Histograms of the amplitude of open events were constructed (10 bins per pA) and fitted with an equation consisting of four Gaussian components;

the mean for each Gaussian component was converted to conductance by dividing by the holding potential (-100 mV). Mean conductance values were compared with one-way or two-way ANOVA (Tukey HSD test). P values < 0.05 were considered statistically significant. Values are reported as mean \pm SEM unless otherwise indicated.

Results

Changes in FRET between the GluA1 C-terminal segment and the plasma membrane

For our FRET investigations into the mechanism of PKC phosphorylation on the AMPA GluA1 channel, we first sought to observe the FRET between the AMPA GluA1 C-Terminus and plasma membrane to determine if the domain lay in proximity to the membrane. We expressed our acceptor RFP-tagged wild type protein with the donor inner leaflet marker Lyn-GFP and TARP γ 2. The emission spectrum with excitation at the donor frequency (420 nm) is shown in Figure 8.

The higher intensity peak at 620 nm (RFP emission peak) for GluA1-RFP with TARP γ 2 in the presence of Lyn-GFP relative to the spectrum of HEK-293 cells with donor-only, indicates that there is basal FRET between GluA1-RFP and Lyn-GFP. The emission spectrum of HEK-293 cells transfected with only the acceptor GluA1-RFP shows no significant RFP intensity at 620 nm upon excitation at 420 nm, showing that there is no significant bleed through due to direct excitation of acceptor, further confirming that the intensity seen in GluA1-RFP with TARP γ 2 and Lyn-GFP expressing cells is due to FRET.

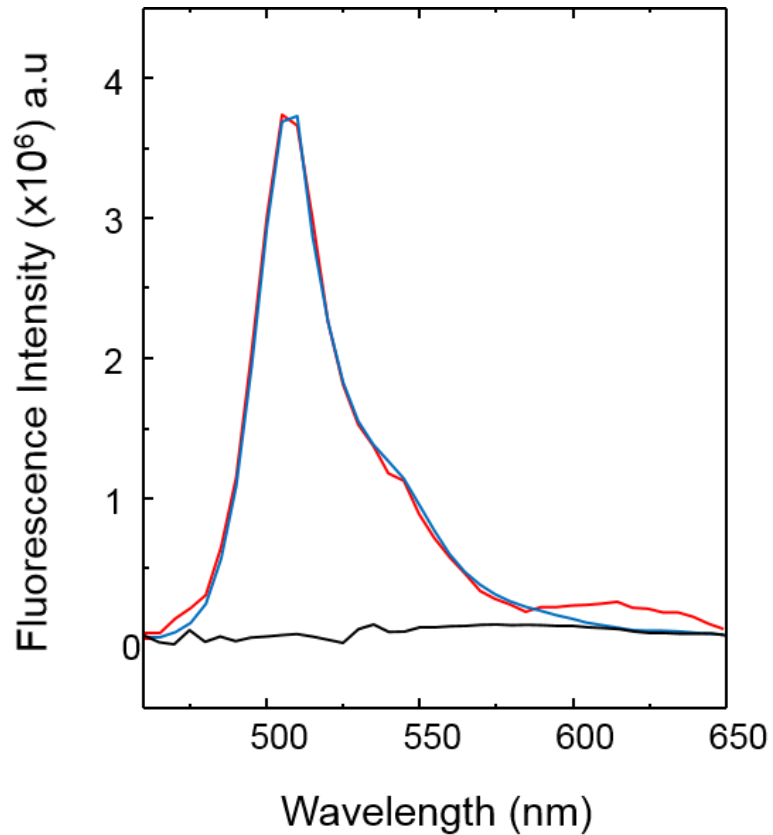


Figure 8. FRET Showing GluA1 Proximity to Inner Leaflet

The GluA1 C-terminal domain tagged with RFP shows FRET with the inner leaflet of the plasma membrane tagged with Lyn-GFP, indicating their relative proximity. Emission spectrum of whole cells is shown expressing GluA1-RFP with TARP $\gamma 2$ in the presence of donor Lyn-GFP (red trace, FRET), versus the donor Lyn-GFP alone (blue trace, no FRET). GluA1-RFP with TARP $\gamma 2$ alone (black, no FRET) with 420 nm excitation.

The precise distance between the two cannot be obtained due to limitations in the method (such as the large size of donor and acceptor). However, the relative changes in the FRET in the different conditions provide insight into motions between the donor and acceptor fluorophores.

Phosphorylation affects channel function, so we next sought to determine what changes in the relative proximity of wild type GluA1 to the plasma membrane are induced by channel activation. We collected the emission spectrum before and after addition of saturating concentrations of glutamate and cyclothiazide. The presence of cyclothiazide stabilizes the open state of the receptor, yielding a homogenous receptor population, and hence allows for a comparison of changes between the Apo and activated state of the protein. (Figure 9). Comparing the emission spectrum in the Apo state (red trace) with that of the predominantly open channel form of the receptor (blue trace), it is evident that there is a concurrent decrease in the donor intensity and increase in the acceptor intensity upon activation.

There is a clear change in the FRET between the receptor and Lyn-GFP; these changes are most evident in the difference spectrum obtained from the spectra in Apo and open conditions measured for the same batch of cells (Figure 9, black trace, Apo minus activated).

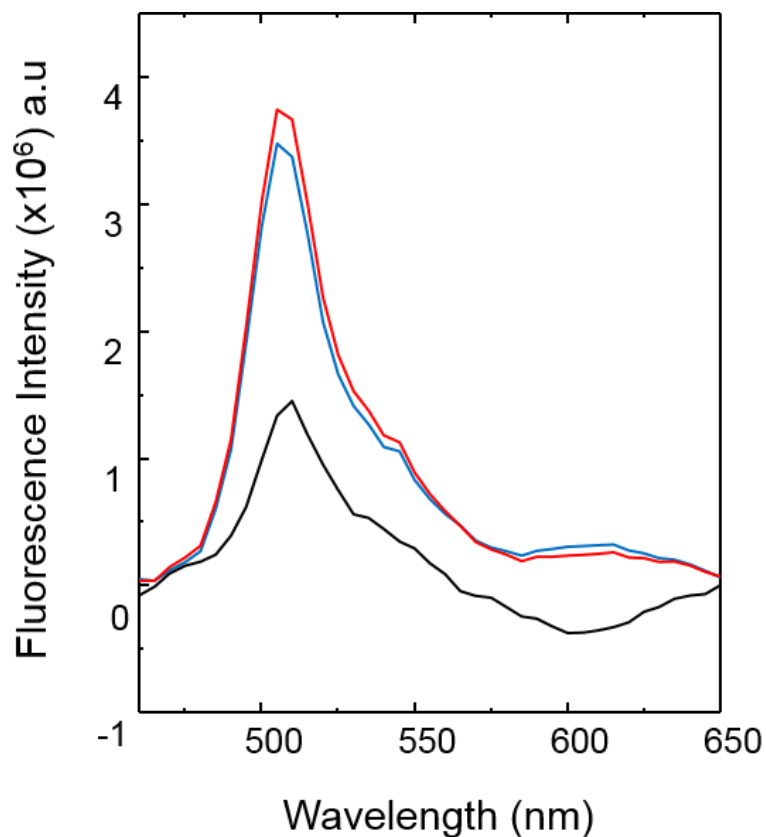


Figure 9. Movement of the GluA1 CD toward the Plasma Membrane Upon Channel Opening

Emission spectrum of whole cells expressing GluA1-RFP with TARP $\gamma 2$ in the presence of donor Lyn-GFP in the Apo state (red trace) and in the presence of 1 mM glutamate and 100 μ M cyclothiazide (blue trace) is shown. The difference between the spectra obtained under Apo and under predominantly open channel conditions (Apo minus activated) is shown below (black), enhanced to 5x for clarity.

To confirm that the observed changes were specifically due to a change in FRET efficiency, we also expressed the donor Lyn-GFP and acceptor GluA1-RFP individually to test their response to activating conditions. Such a change is not observed in either the donor-only or the acceptor-only emission spectrum (Figure 10, solid vs dashed traces), further confirming that the change is due to a change in FRET efficiency. The increase in FRET upon addition of glutamate and cyclothiazide indicates a decrease in distance between the fluorophores, thus, between the receptor domain and Lyn. These data suggest that the C-terminal segment moves towards the inner leaflet of plasma membrane upon activation of the receptor.

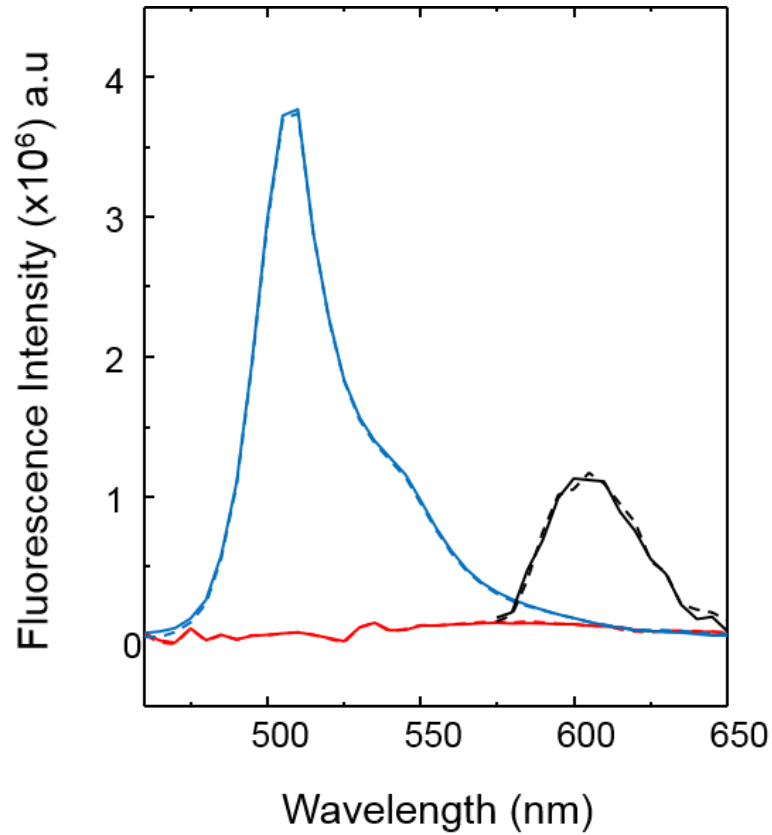


Figure 10. Lack of Change in Fluorescent Cells Expressing Donor only and Acceptor only

Emission spectrum of whole cells expressing GluA1-RFP with TARP $\gamma 2$ (red traces) and Lyn-GFP (blue traces) with 420 nm excitation in apo (solid traces) and primarily open in presence of 1 mM glutamate and 100 μ M cyclothiazide (dashed traces) for, and for GluA1-RFP with TARP $\gamma 2$ with 550 nm excitation (black trace).

Having confirmed basal FRET and an activation-induced increase in FRET in the receptor, we then investigated the changes in these qualities induced by PKC phosphorylation. We mimicked phosphorylation in the domain by using glutamate substitutions at S818, S831, and T840 to make a triple mutant, GluA1P-RFP. We co-expressed the phosphomimetic GluA1P-RFP receptor with TARP γ 2 and Lyn-GFP and collected emission spectra with the same protocol as with the wild type to investigate basal FRET. The GluA1P-RFP (black trace) is compared to that of GluA1-RFP receptor with TARP γ 2 and Lyn-GFP (red trace) in Figure 11. The lower intensity at the acceptor emission wavelength (620 nm) for the cells expressing the phosphomimetic GluA1P-RFP receptor indicates lower FRET. This reduction FRET in turn can be correlated to a longer distance between RFP and Lyn-GFP in the phosphomimetic GluA1 receptor relative to the wild type receptor.

To determine if, there was any change in FRET induced by activation in the phosphomimetic GluA1P-RFP, a difference spectrum was obtained between the emission spectrum in the absence and presence of saturating concentrations of glutamate and cyclothiazide (Figure 12). The difference spectrum (black trace) is essentially flat, a strong indication that receptor activation does not lead to significant changes in the distance between the C-terminus and the inner leaflet of the plasma membrane for the phosphomimetic GluA1 receptor. The results of the wild-type GluA1-RFP and phosphomimetic GluA1-RFP were compared to the triple alanine phosphodeficient GluA1A-RFP (Figure 12, blue).

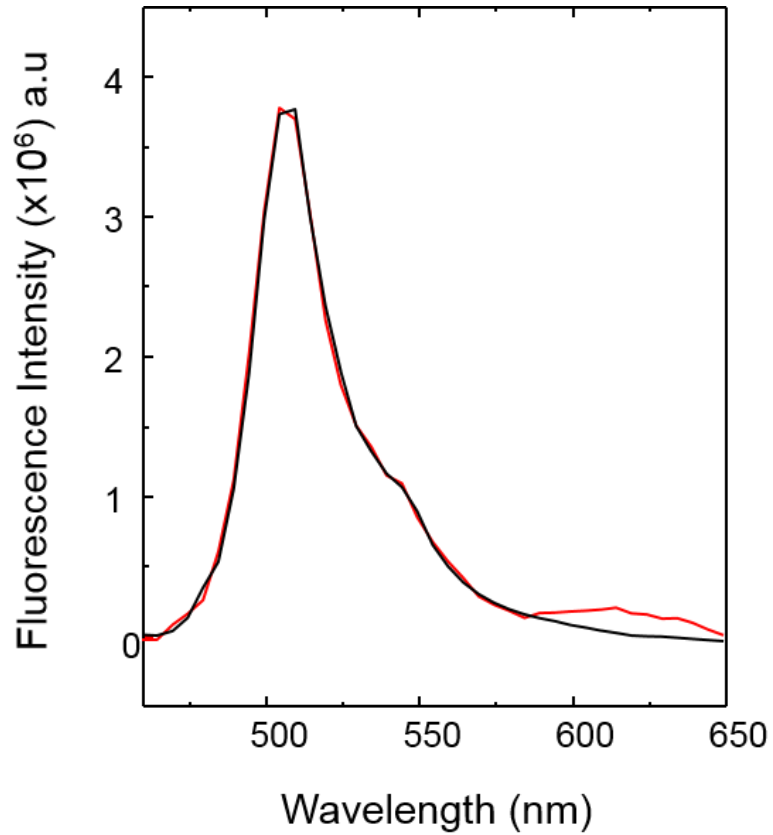


Figure 11. Lower FRET between GluA1 CTD and Lyn-GFP at the Plasma Membrane upon Phosphorylation

Emission spectrum of whole cells expressing GluA1-RFP (red trace) and phosphomimetic GluA1P-RFP (black trace) both in the presence of TARP $\gamma 2$ and donor Lyn-GFP at excitation 420 nm. The phosphomimetic mutant exhibits reduced RFP emission (620 nm) relative to GluA1-RFP.

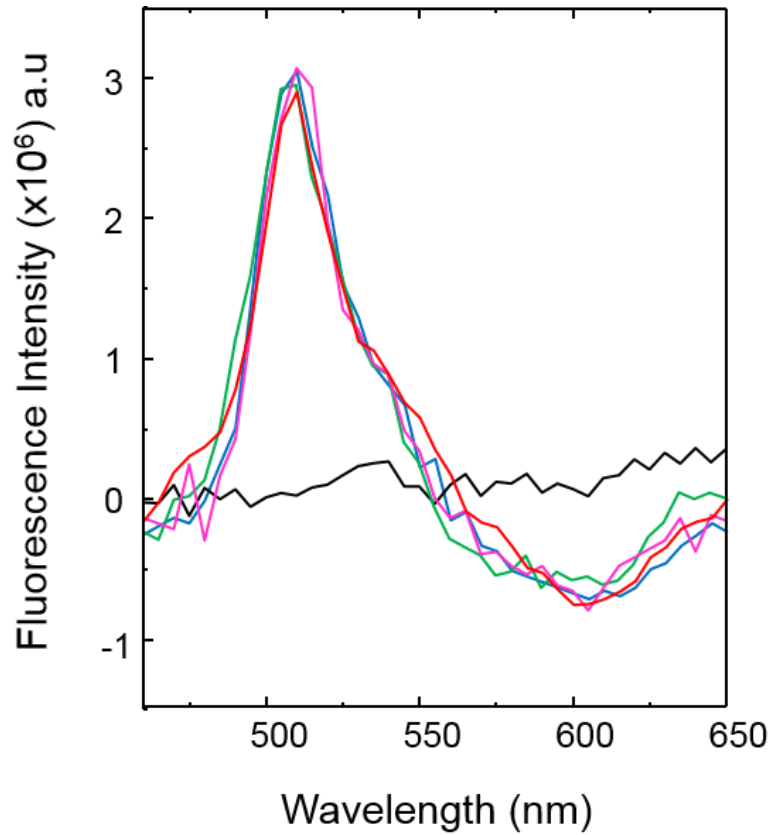


Figure 12. Phosphorylation Eliminates Activation-Induced Changes in FRET and is Restored by Positive Lipid

Difference spectra (Apo minus activated) are shown for GluA1-RFP (red), GluA1P-RFP (black), phosphodeficient GluA1A-RFP (blue), GluA1-RFP with sphingosine addition (green), and the restored GluA1P-RFP with sphingosine addition (magenta).

The difference spectrum for the phosphodeficient GluA1-RFP was similar to that obtained with the wild-type GluA1-RFP receptor, indicating that the wild type receptor is predominantly dephosphorylated in these experiments (not shown).

Effect of local membrane charge on the position of the GluA1 C-terminal segment

Given that our FRET data indicate that the C-terminal domain is in close physical proximity to the inner surface of the membrane leaflet, and since the inner leaflet has a significant fraction of lipids with negatively charged headgroups in mammalian cells, we next tested the effect of changing the net charge of the lipid leaflet on the motions of the GluA1 C-terminal segment. We reduced the endogenous negative charge in HEK cells along the membrane incorporating sphingosine, a positively charged lipid, into the membrane prior to the FRET measurement (86, 93). Treatment with sphingosine had no effect on the FRET signals for the pattern of activation-induced FRET in the phosphodeficient receptor (Figure 12, compare blue and green). In contrast, altering the charge on the inner leaflet rescued wild type behavior of activation-induced FRET in the more negatively charged phosphomimetic receptor, and the difference spectrum (magenta) was similar to that seen for the wild-type and phosphodeficient receptor (Figure 12). These experiments verified that the mechanism by which phosphorylation alters the motion of the C-Terminus relative to the plasma membrane is dependent on lipid charge environment, and can be eliminated depending on the local composition of lipid charge.

Imaging based FRET measurements

One limitation of the ensemble FRET technique is the potential for internal receptors (those not inserted into the plasma membrane) to fluoresce upon excitation and contribute to the basal fluorescence spectrum. However, these would not contribute to the activation-induced change in the emission spectrum since only surface-expressed receptors activate due to the addition of extracellular agonist. In order to narrow our results to the plasma membrane and to verify our ensemble measurements we obtained images of single cells expressing GluA1-RFP with TARP $\gamma 2$ and Lyn-GFP and determined FRET for defined regions at the plasma membrane. Figure 13A shows representative images of the cells. Consistent with the ensemble measurements, the phosphodeficient GluA1-RFP showed increased FRET upon activation by 1 mM glutamate and 100 μ M cyclothiazide, with no substantive change upon sphingosine treatment as expected (Figure 13C). The Apo states of the receptors showed a pattern similar to what we saw in the ensemble experiments, with phosphodeficient proteins exhibiting a higher ratio (FRET/Donor) compared to the phosphoprotein (Figure 13B). Phosphomimetic receptors showed no change upon activation, but activation-induced FRET was recovered in the sphingosine-treated cells (Figure 13C).

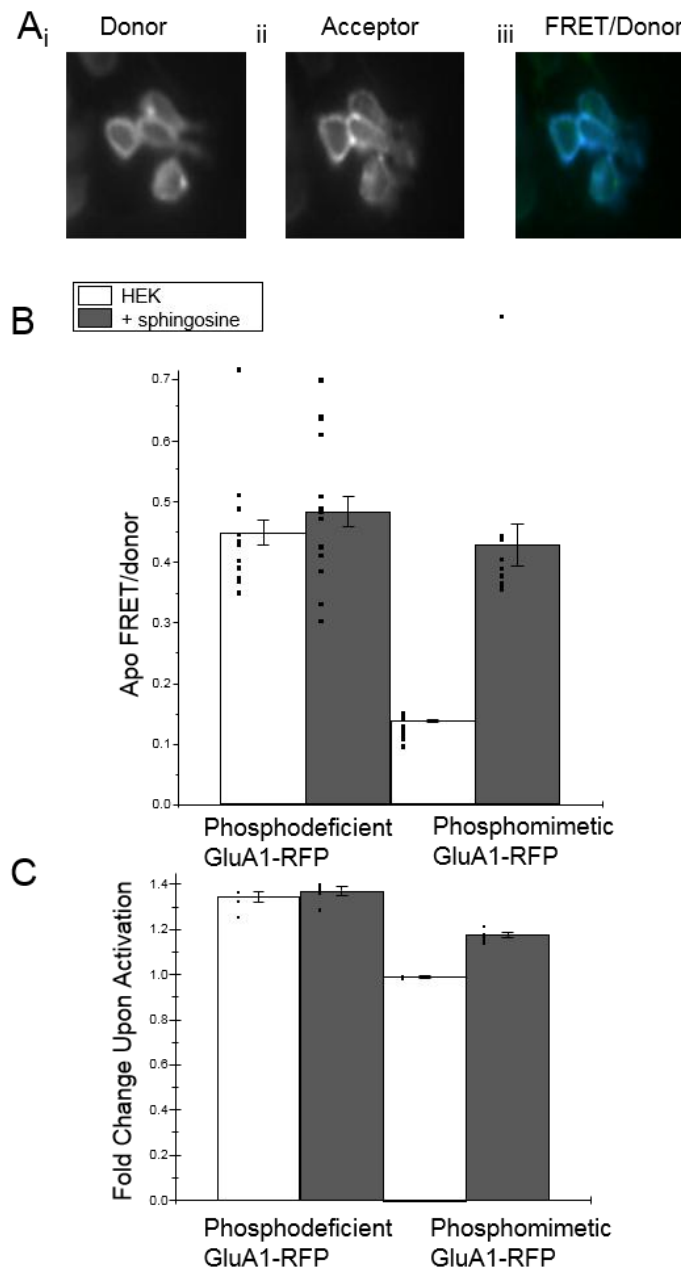


Figure 13. Single Cell Imaging Verifies FRET Change due to Phosphorylation.

A) Representative images of cells expressing GluA1-RFP and Lyn-GFP with donor excitation (left), acceptor excitation (center), and FRET signal (FRET/Donor) (right). B) Bar graphs showing FRET signal (FRET/Donor) from plasma membrane segments of cells. Bars represent N=15, 16, 20, and 15 cells

(left to right) cells selected for plasma membrane signal analysis, with S.E.M. visualized as an error bar. C) Bar graphs representing single cell measurements for activation-induced FRET change (FRET/donor fold change upon activation by 1 mM glutamate and 100 μ M cyclothiazide). For these data, each bar is N=5 with error bars as S.E.M. Individual data points are overlaid. All FRET signals are reported as FRET/Donor to account for potential bleedthrough. All experiments were repeated in at least triplicate.

Together with our ensemble FRET measurements, the data for cell surface receptors support a mechanism in which PKC phosphorylation causes a repulsive interaction between the GluA1 carboxy-terminal domain and the plasma membrane, which is removed by either eliminating the phosphorylation or reducing the negative charge of phospholipids along the inner leaflet.

The effect of PKC phosphorylation and lipid composition on GluA1 function at the single-channel conductance

Previous work has shown that phosphorylation at the three C-terminal PKC sites increases the average unitary conductance of GluA1 receptors (28, 29, 50). Our FRET-based data would suggest that elimination of this effect should be achievable by altering the charge environment along the inner leaflet. To functionally verify this hypothesis, single-channel currents were recorded in outside-out patches from cells expressing phosphomimetic GluA1P and the results compared with those for wild-type GluA1. Both GluA1 constructs were co-expressed with TARP $\gamma 2$.

Figure 14 shows examples of unitary currents recorded in these experiments. The currents were evoked at -100 mV by the continuous application of 10 mM glutamate. Columns A and B show unitary currents through wild-type GluA1 receptors and GluA1 phosphomimetic receptors with normal internal solution (no charge alteration). Four open levels (subconductance states) were detected in each of the patches analyzed, as expected in AMPA receptors.

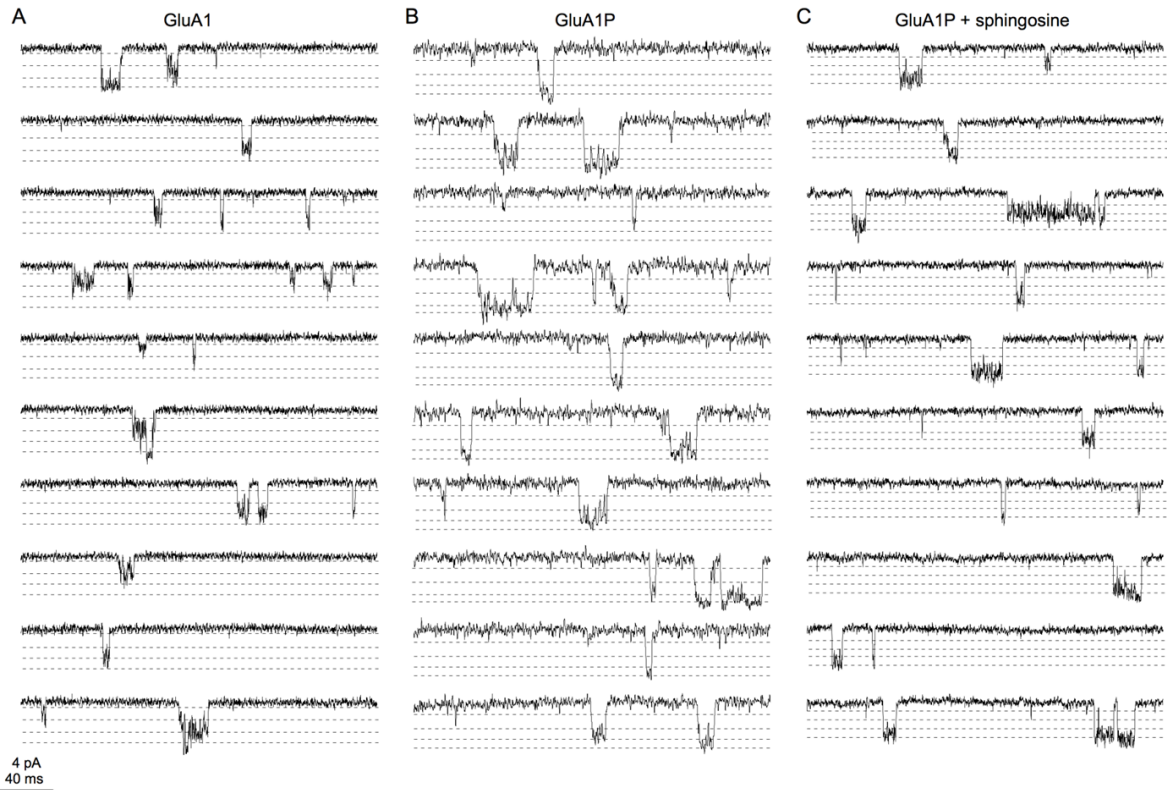


Figure 14. AMPA Receptor Unitary Conductance Influenced by Interactions with Inner Leaflet of Plasma Membrane

Examples of unitary AMPA receptor currents evoked at -100 mV by the continuous application of 10 mM glutamate in outside-out patches from cells transfected with TARP $\gamma 2$ and either wild-type GluA1 (A) or the GluA1 phosphomimetic mutant (GluA1P; B and C). Dashed lines in each column indicate the current values corresponding to the four open levels detected in the patch, which were obtained from multiple-Gaussian fits to amplitude distributions of several hundred events. The data shown for the phosphomimetic mutant (B and C) are from recordings with cells without and with pre-incubation with sphingosine (100 μ M).

The individual subconductance levels (O1, O2, O3 and O4), which were obtained from multiple Gaussian fits to amplitude distributions of hundreds of single-channel events (see Methods Specific to this Section), are indicated by the dashed traces in each panel of Figure 14. Each of the four open levels was 15-40% larger for the phosphomimetic GluA1 receptors (GluA1P) than for wild-type GluA1. Figure 14C shows representative data obtained from a patch excised from a cell expressing TARP $\gamma 2$ and the GluA1 phosphomimetic that was pre-exposed to 100 μ M sphingosine. The currents and conductance levels seen in this patch were recovered to the corresponding data for wild-type receptors. Similar data that were suitable for detailed analysis were obtained with sphingosine and phosphomimetic GluA1 from one additional patch. The conductance levels measured in these patches were not significantly different from the levels measured for GluA1 wild-type, but both sets of open levels were significantly smaller than the levels measured for phosphomimetic GluA1 receptors without pre-exposure to sphingosine ($P < 0.01$, two-way ANOVA). Thus, reducing the net negative charge on the inner leaflet by incorporating sphingosine into the inner leaflet prevents the increase in unitary conductance seen for the phosphomimetic GluA1 mutant receptor.

The outside-out configuration used to record the unitary GluA1 receptor currents affords direct access to the inner leaflet of the plasma membrane. To test further our hypothesis that electrostatic interactions with negatively charged head groups on the inner leaflet play a key role in the increased conductance seen with phosphomimetic GluA1 receptors, we screened these interactions by

including poly-L-lysine, a small poly cation, into the pipette solution and comparing the single channel data for wild-type GluA1 and GluA1P mutant receptors to the results obtained with control pipette solution. As in all the patch-clamp experiments, the pipette solution did not contain ATP or any other substrate for phosphorylation. Representative amplitude histograms for the phosphomimetic mutant GluA1P with (Figure 15B) and without (Figure 15A) the addition of poly-L-lysine (PK) to the pipette solution are shown in Figure 15. As can be seen, the unitary conductance for each of the four open levels is substantially smaller for the GluA1P mutant when inner leaflet charge was screened.

Figure 15C shows the mean data obtained for the four different conditions tested (wild-type or mutant GluA1 with TARP $\gamma 2$ receptors, with and without reducing surface charge on the internal membrane leaflet). Each of the four open levels observed for the GluA1 mutant receptors with normal internal solution in the recording pipette was significantly larger than the corresponding values seen for wild-type GluA1 or mutant GluA1 receptors with poly-L-lysine in the pipette when the data were compared with a two-way ANOVA ($P < 0.01$). The absolute difference in unitary conductance was smallest for O1, but when the results for the four groups were expressed as the percentage difference from the mean value for wild-type receptors with normal internal solution, the difference seen for the mutant receptors was biggest for the smallest open level, O1, and inversely correlated with the absolute conductance of the four sublevels (inset in Figure 15C).

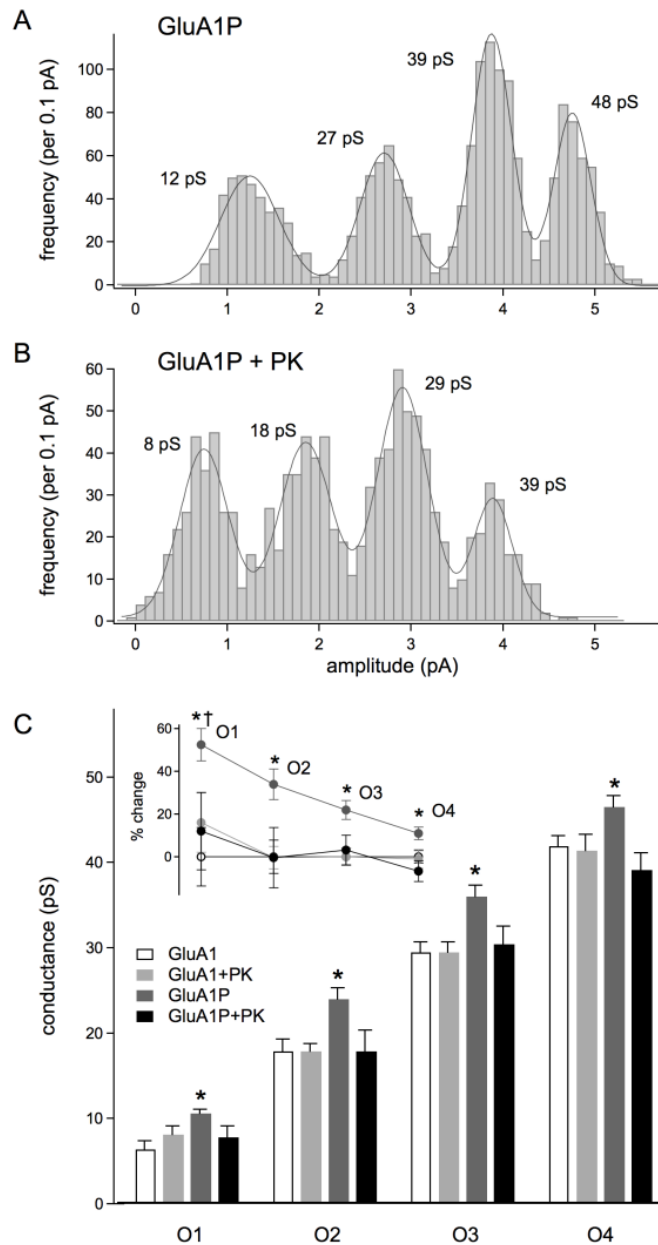


Figure 15. Screening C-terminal Membrane Interactions Prevents Phosphorylation-Induced Increase in Unitary Current

A, B. Amplitude histograms for inward unitary currents from two patches for GluA1P/TARP γ -2 receptors without (A) or with (B) poly-L-lysine (PK) added to the pipette solution. Currents were recorded during the continuous application of

10 mM glutamate. Data was fitted to 4 Gaussians (solid trace). Conductance estimates for the four open levels obtained from the fit are indicated in each panel. C. Bar graph illustrating the mean conductance values obtained for each open level under the four conditions tested (GluA1 or GluA1P, with or without poly-L-lysine). Individual conductance values were obtained from 4-Gaussian fits to amplitude histograms for each patch (3-6 patches per group). The conductance values obtained for GluA1P without addition of poly-L-lysine to the pipette solution were significantly greater than the corresponding values for the other three groups (* $P < 0.01$, two-way ANOVA). Inset shows the mean change relative to control values for each of the four open levels. The values for the GluA1P mutant differ significantly from the corresponding values for the other three groups and the O1 mean for the GluA1 phosphomimetic was significantly different from the mean change values for O3 and O4 (one-way ANOVA, * $P < 0.01$; $^{\dagger} P < 0.05$).

In previous work (50), C-terminal phosphomimetic mutations in GluA1 were shown to increase the proportion of openings to the larger subconductance levels (O3 and O4) without significantly altering the conductance of the different open levels. Because we co-expressed the mutant receptors with the auxiliary subunit TARP $\gamma 2$, we cannot directly compare our data with these previous results. The proportion of openings to O3 and O4 was larger for the GluA1P receptors (normal internal), but the difference did not reach statistical significance. To account for this additional, albeit modest effect, we calculated the weighted mean unitary current for each of the groups by multiplying the relative area for each open level and the mean current for that level (values obtained from the 4-Gaussian fits to the amplitude histograms). To increase the power of the comparison, the sphingosine and poly-L-lysine data were pooled. The mean unitary current (at -100 mV holding) obtained in this way for the GluA1P receptors (2.81 ± 0.21 pA, $N = 5$) was larger than the corresponding values for wild-type receptors (2.10 ± 0.21 pA and 1.92 ± 0.12 pA without and with poly-L-lysine or sphingosine, respectively; $N = 6$ and 5 patches) or mutant receptors under conditions where internal surface charge was reduced (2.17 ± 0.22 pA, $n = 5$). The means for GluA1P without charge screening and wild-type GluA1 with charge screening were statistically significant (one-way ANOVA, $P < 0.05$), and the size of the increase in the weighted unitary current for the phosphomimetic mutant compared with the other three groups (30-46%) agrees well with results obtained previously for GluA1 with TARP $\gamma 2$ receptors from stationary noise analysis (50).

Discussion

The cytoplasmic carboxy-termini of AMPA receptors convey trafficking and regulatory properties in a subunit-specific manner. The GluA1 C-terminal domain promotes targeting, trafficking, as well as stable protein interactions with the cytoskeleton at the synapse. Phosphorylation in this domain had been previously shown to affect trafficking through phosphorylation at site S845, and PKC phosphorylation at sites S818, S831 and T840 has been shown to increase channel conductance (19, 28, 29, 50, 94). We used multiple biophysical techniques to examine the mechanism of this functional modulation, based upon the hypothesis that a physical shift relative to the plasma membrane occurred due to phosphorylation (hypothesis based on data presented in Chapter 3).

Our ensemble and single cell FRET data support a mechanism of action in which PKC phosphorylation alters direct charge interactions between the membrane and the GluA1 C-terminal domain. The wild type receptor-and similarly behaved phosphodeficient receptor-show a clear activation-induced shift in FRET indicating increased membrane proximity, which is absent in the phosphomimetic protein. This argues in favor of a mechanism by which the wild-type protein shifts to accommodate channel opening and avoids affecting channel conductance, whereas the phosphoprotein does not and thereby affects channel activity. The rescue of wild type behavior in receptors with decreased negativity along the plasma membrane establishes the electrostatic basis of PKC phosphorylation's functional effect on AMPA GluA1.

Our patch-clamp results support previous data demonstrating an effect of phosphorylation of C-terminal residues on the unitary conductance of AMPA receptors (50). Unlike the prior work, we found that the absolute conductance values associated with each of the four subconductance states were significantly increased. It is important to note, however, that our data do not contradict directly the data of Kristensen and colleagues (2011), who found that introducing a phosphomimetic mutation at GluA1 S831 increased the frequency of large-conductance openings without altering the conductance values of the different subconductance levels. Our single-channel results were obtained for wild-type and the GluA1P receptors with auxiliary subunit TARP $\gamma 2$, whereas the earlier single-channel data were obtained in the absence of TARPs. The inclusion of TARP $\gamma 2$ in receptor assemblies itself shifts the relative occupancy of the four open levels toward larger-conductance states (90, 94), which may limit or mask any additional effect of C-terminal mutations. TARPs are also known to alter rectification behavior and directly affect ion permeation (48, 95-97). Indeed, we did see some effect on the relative occupancy of the four open levels with the phosphomimetic mutant. For example, openings to O4 in normal internal solution were more frequent for GluA1P-containing receptors than for receptors with wild-type GluA1. In total, however, the differences did not reach statistical significance. As noted in the Results, the percentage increase in the weighted mean single-channel current we found here for the GluA1 phosphomimetic mutant is in excellent agreement with the increase in the apparent unitary current

estimated previously from noise analysis when TARP 2 was co-transfected with GluA1 (29, 50).

Our findings provide strong indications that the effect on unitary conductance we observed here for the GluA1 phosphomimetic mutant is directly related to electrostatic interactions with negatively charged phospholipid head groups on the internal membrane leaflet. When these charges were reduced by pre-exposure of the cells to sphingosine or screened by including poly-L-lysine in the pipette solution, the conductance values obtained for each of the four open levels were indistinguishable from receptors that contained wild-type GluA1. Inclusion of poly-L-lysine in the pipette or pre-exposure to sphingosine had no effect on the conductance of wild-type GluA1-containing receptors, arguing against an independent effect of these treatments on unitary conductance. Interestingly, although the absolute change in unitary conductance was greatest for the largest open level, O4, the percentage change in conductance was largest for O1 and scaled inversely with the amplitude of the subconductance states (Figure 15C). This result would appear to be unexpected if the effect of altering C-terminal or membrane charge resulted from changes in the local concentration of permeant ions near the pore. Together with our FRET data, which indicate that the functional changes in unitary conductance are associated with changes in the conformation of the GluA1 C-terminus, the patch-clamp results seem most consistent with the conclusion that the conformation of the C-terminus can have a direct effect on the conformation of the conductance pathway itself, perhaps changing the height of an energy barrier to ion permeation. Given the known

correlation between receptor occupancy and the likelihood of openings to the various substates (98, 99), this effect of the GluA1 C-terminus would appear to scale inversely with the number of subunits contributing to activation gating. The allosteric effect of phosphorylation-mediated position shifts in the C-terminus may therefore be of greatest consequence at glutamate concentrations where receptor occupancy is low.

The strong correlation between our FRET results and the single-channel data indicate that phosphorylation of sites in the C-terminus of AMPA receptor core subunits shifts the C-terminus away from the membrane, which in turn alters the rate of ion flux through the pore. Our data support the idea that the position shift is the result of direct charge-charge interactions between the phosphorylated C-terminus and the membrane inner leaflet, suggesting the possibility that changes in the lipid composition or charge of the plasma membrane could influence phosphorylation-mediated changes in AMPA receptor function.

One remaining question from these studies is precisely how the changes in the C-terminus of AMPA GluA1 physically translate to altered ion flux, and multiple mechanisms acting either singularly or in concert can be considered. A clear potential answer lies in the simple notion that phosphorylation, or glutamate substitution, alters the local charge environment of the intracellular side of the pore, thereby changing the charge gradient affecting ions traveling through the channel. For a hydrated channel without restrictive gating, this would seem to be the obvious mechanism of choice. However, glutamate receptors possess

complex gating properties, which work in concert to move dehydrated ions through multiple pockets in the permeation pathway. The properties (degree of steric/charge restriction to hold the ion in place) of these pockets are dictated by the side chains of nearby amino acids. The shifting of these side chains in the transmembrane domain due to post-translational modifications in another domain is a distinct possibility, and these shifts may alter the environment of ions as they move through the channel. Precedent for the importance of steric and charge environment in the channel pore can be appreciated by an examination of potassium channels, which share demonstrably similar topology to iGluRs (100-102). This family of cation channels have gating properties which regulate the flow of dehydrated ions through their pore. They possess not only a canonical five-amino acid motif at their narrowest point, known as the selectivity filter, but also multiple other sites which stabilize the filter and regulate ion flow through the channel by creating vestibules where potassium ions are stabilized within the pore (103, 104). Mutations within the pore of both potassium channels and iGluRs have been shown to significantly affect ion flux (105-107). It follows that shifts within the domain translated from post-translational modifications like phosphorylation in the C-terminus could greatly affect flux as well.

DISCUSSION - FINAL THOUGHTS & FUTURE DIRECTIONS

Future Directions

The most novel aspect of this work verified that phosphorylation by protein kinase C (mimicked with glutamate substitutions in this work) negates an activation-induced domain shift that occurs in wild type protein, and in fact shifts the domain away from the membrane at the basal level, prior to the channel opening. This mechanism is dependent on lipid charge environment as shown in the cells with altered inner leaflet charge, which showed recovery to wild type behavior. Future studies could expand our understanding by investigating how and which lipids may be functioning as regulators of AMPA receptors at the synapse (for instance, if lipid composition changes are induced specifically to shepherd receptors into clusters or to increase the probability of membrane insertion or recycling). These studies could use lipid-specific markers to investigate precise lipid content at the synapse in order to expand our understanding of the AMPA receptor's extensive regulatory pathways.

Final Thoughts

These studies constitute a step toward our understanding of the significance and potential therapeutic use of carboxy-terminal domains in membrane receptors. As more information is garnered from these functionally significant yet largely discounted domains, the biomedical field will move closer to an enlightened understanding of neuronal activity.

Works Cited

1. Kuffler, S. W., and C. Edwards. 1958. Mechanism of gamma aminobutyric acid (GABA) action and its relation to synaptic inhibition. *J Neurophysiol* 21: 589-610.
2. Sieghart, W., K. Fuchs, V. Tretter, V. Ebert, M. Jechlinger, H. Höger, and D. Adamiker. 1999. Structure and subunit composition of GABA(A) receptors. *Neurochem Int* 34: 379-385.
3. Sieghart, W., and G. Sperk. 2002. Subunit composition, distribution and function of GABA(A) receptor subtypes. *Curr Top Med Chem* 2: 795-816.
4. Hollmann, M., and S. Heinemann. 1994. Cloned glutamate receptors. *Annual Review of Neuroscience* 17: 31-108.
5. Nakanishi, S., and M. Masu. 1994. Molecular diversity and functions of glutamate receptors. *Annual Reviews in Biophysical and Biomolecular Structure* 23: 329-348.
6. Dingledine, R., K. Borges, D. Bowie, and S. F. Traynelis. 1999. The glutamate receptor ion channels. *Pharmacological Reviews* 51: 7-61.
7. Riedel, G., B. Platt, and J. Micheau. 2003. Glutamate receptor function in learning and memory. *Behav Brain Res* 140: 1-47.
8. Suzuki, T., K. Tsuzuki, K. Kameyama, and S. Kwak. 2003. Recent advances in the study of AMPA receptors. *Nippon Yakurigaku Zasshi* 122: 515-526.
9. Bergink, V., H. J. van Megen, and H. G. Westenberg. 2004. Glutamate and anxiety. *Eur Neuropsychopharmacol* 14: 175-183.

10. Mosbacher, J., R. Schoepfer, H. Monyer, N. Burnashev, P. H. Seeburg, and J. P. Ruppersberg. 1994. A molecular determinant for submillisecond desensitization in glutamate receptors. *Science* 266: 1059-1062.
11. Edmonds, B., A. J. Gibb, and D. Colquhoun. 1995. Mechanisms of activation of glutamate receptors and the time course of excitatory synaptic currents. *Annu Rev Physiol* 57: 495-519.
12. Jonas, P., and N. Spruston. 1994. Mechanisms shaping glutamate-mediated excitatory postsynaptic currents in the CNS. *Curr Opin Neurobiol* 4: 366-372.
13. Monyer, H., R. Sprengel, R. Schoepfer, A. Herb, M. Higuchi, H. Lomeli, N. Burnashev, B. Sakmann, and P. H. Seeburg. 1992. Heteromeric NMDA receptors: molecular and functional distinction of subtypes. *Science* 256: 1217-1221.
14. Vicini, S., J. F. Wang, J. H. Li, W. J. Zhu, Y. H. Wang, J. H. Luo, B. B. Wolfe, and D. R. Grayson. 1998. Functional and pharmacological differences between recombinant N-methyl-D-aspartate receptors. *J Neurophysiol* 79: 555-566.
15. Burnashev, N., R. Schoepfer, H. Monyer, J. P. Ruppersberg, W. Günther, P. H. Seeburg, and B. Sakmann. 1992. Control by asparagine residues of calcium permeability and magnesium blockade in the NMDA receptor. *Science* 257: 1415-1419.

16. Hume, R. I., R. Dingledine, and S. F. Heinemann. 1991. Identification of a site in glutamate receptor subunits that controls calcium permeability. *Science* 253: 1028-1031.
17. Verdoorn, T. A., N. Burnashev, H. Monyer, P. H. Seeburg, and B. Sakmann. 1991. Structural determinants of ion flow through recombinant glutamate receptor channels. *Science* 252: 1715-1718.
18. Sobolevsky, A. I., M. P. Rosconi, and E. Gouaux. 2009. X-ray structure, symmetry and mechanism of an AMPA-subtype glutamate receptor. *Nature* 462: 745-756.
19. Banke, T. G., D. Bowie, H. K. Lee, R. L. Huganir, A. Schousboe, and S. F. Traynelis. 2000. Control of GluR1 AMPA Receptor Function by cAMP-Dependent Protein Kinase. *The Journal of Neuroscience* 20: 89-102.
20. Derkach, V., A. Barria, and T. R. Soderling. 1999. Ca²⁺/calmodulin-kinase II enhances channel conductance of alpha-amino-3-hydroxy-5-methyl-4-isoxazolepropionate type glutamate receptors. *Proceedings of the National Academy of Sciences of the United States of America* 96: 3269-3274.
21. Poncer, J. C., J. A. Esteban, and R. Malinow. 2002. Multiple mechanisms for the potentiation of AMPA receptor-mediated transmission by alpha-Ca²⁺/calmodulin-dependent protein kinase II. *The Journal of neuroscience : the official journal of the Society for Neuroscience* 22: 4406-4411.

22. Malinow, R., and R. C. Malenka. 2002. AMPA receptor trafficking and synaptic plasticity. *Annual review of neuroscience* 25: 103-126.
23. Esteban, J. A., S. H. Shi, C. Wilson, M. Nuriya, R. L. Huganir, and R. Malinow. 2003. PKA phosphorylation of AMPA receptor subunits controls synaptic trafficking underlying plasticity. *Nature neuroscience* 6: 136-143.
24. Hayashi, T., G. Rumbaugh, and R. L. Huganir. 2005. Differential regulation of AMPA receptor subunit trafficking by palmitoylation of two distinct sites. *Neuron* 47: 709-723.
25. Cooper, D. R., D. M. Dolino, H. Jaurich, B. Shuang, S. Ramaswamy, C. E. Nurik, J. Chen, V. Jayaraman, and C. F. Landes. 2015. Conformational transitions in the glycine-bound GluN1 NMDA receptor LBD via single-molecule FRET. *Biophysical journal* 109: 66-75.
26. Ramaswamy, S., D. Cooper, N. Poddar, D. M. MacLean, A. Rambhadran, J. N. Taylor, H. Uhm, C. F. Landes, and V. Jayaraman. 2012. Role of conformational dynamics in alpha-amino-3-hydroxy-5-methylisoxazole-4-propionic acid (AMPA) receptor partial agonism. *The Journal of biological chemistry* 287: 43557-43564.
27. Dolino, D. M., D. Cooper, S. Ramaswamy, H. Jaurich, C. F. Landes, and V. Jayaraman. 2015. Structural dynamics of the glycine-binding domain of the N-methyl-D-aspartate receptor. *The Journal of biological chemistry* 290: 797-804.

28. Jenkins, M. A., and S. F. Traynelis. 2012. PKC phosphorylates GluA1-Ser831 to enhance AMPA receptor conductance. *Channels (Austin)* 6: 60-64.
29. Jenkins, M. A., G. Wells, J. Bachman, J. P. Snyder, A. Jenkins, R. L. Huganir, R. E. Oswald, and S. F. Traynelis. 2014. Regulation of GluA1 alpha-amino-3-hydroxy-5-methyl-4-isoxazolepropionic acid receptor function by protein kinase C at serine-818 and threonine-840. *Mol Pharmacol* 85: 618-629.
30. Hu, G. Y., O. Hvalby, S. I. Walaas, K. A. Albert, P. Skjeflo, P. Andersen, and P. Greengard. 1987. Protein kinase C injection into hippocampal pyramidal cells elicits features of long term potentiation. *Nature* 328: 426-429.
31. Barria, A., V. Derkach, and T. Soderling. 1997. Identification of the Ca²⁺/calmodulin-dependent protein kinase II regulatory phosphorylation site in the alpha-amino-3-hydroxyl-5-methyl-4-isoxazole-propionate-type glutamate receptor. *The Journal of biological chemistry* 272: 32727-32730.
32. Roche, K. W., R. J. O'Brien, A. L. Mammen, J. Bernhardt, and R. L. Huganir. 1996. Characterization of multiple phosphorylation sites on the AMPA receptor GluR1 subunit. *Neuron* 16: 1179-1188.
33. Silva, A. J., C. F. Stevens, S. Tonegawa, and Y. Wang. 1992. Deficient hippocampal long-term potentiation in alpha-calcium-calmodulin kinase II mutant mice. *Science (New York, N.Y.)* 257: 201-206.

34. Barria, A., D. Muller, V. Derkach, L. C. Griffith, and T. R. Soderling. 1997. Regulatory phosphorylation of AMPA-type glutamate receptors by CaM-KII during long-term potentiation. *Science (New York, N.Y.)* 276: 2042-2045.
35. Mammen, A. L., K. Kameyama, K. W. Roche, and R. L. Huganir. 1997. Phosphorylation of the alpha-amino-3-hydroxy-5-methylisoxazole4-propionic acid receptor GluR1 subunit by calcium/calmodulin-dependent kinase II. *The Journal of biological chemistry* 272: 32528-32533.
36. Ouyang, Y., A. Rosenstein, G. Kreiman, E. M. Schuman, and M. B. Kennedy. 1999. Tetanic stimulation leads to increased accumulation of Ca(2+)/calmodulin-dependent protein kinase II via dendritic protein synthesis in hippocampal neurons. *The Journal of neuroscience : the official journal of the Society for Neuroscience* 19: 7823-7833.
37. Ramakers, G. M., D. D. Gerendasy, and P. N. de Graan. 1999. Substrate phosphorylation in the protein kinase Cgamma knockout mouse. *The Journal of biological chemistry* 274: 1873-1874.
38. Boehm, J., M. G. Kang, R. C. Johnson, J. Esteban, R. L. Huganir, and R. Malinow. 2006. Synaptic incorporation of AMPA receptors during LTP is controlled by a PKC phosphorylation site on GluR1. *Neuron* 51: 213-225.
39. Lee, H. K., K. Takamiya, K. Kameyama, K. He, S. Yu, L. Rossetti, D. Wilen, and R. L. Huganir. 2007. Identification and characterization of a novel phosphorylation site on the GluR1 subunit of AMPA receptors. *Mol Cell Neurosci* 36: 86-94.

40. Lin, D. T., Y. Makino, K. Sharma, T. Hayashi, R. Neve, K. Takamiya, and R. L. Huganir. 2009. Regulation of AMPA receptor extrasynaptic insertion by 4.1N, phosphorylation and palmitoylation. *Nat Neurosci* 12: 879-887.
41. Lu, W., K. Isozaki, K. W. Roche, and R. A. Nicoll. 2010. Synaptic targeting of AMPA receptors is regulated by a CaMKII site in the first intracellular loop of GluA1. *Proceedings of the National Academy of Sciences* 107: 22266-22271.
42. Prieto, M. L., and L. P. Wollmuth. 2010. Gating modes in AMPA receptors. *The Journal of neuroscience : the official journal of the Society for Neuroscience* 30: 4449-4459.
43. Weber, T., M. A. Vogt, S. E. Gartside, S. M. Berger, R. Lujan, T. Lau, E. Herrmann, R. Sprengel, D. Bartsch, and P. Gass. 2015. Adult AMPA GLUA1 receptor subunit loss in 5-HT neurons results in a specific anxiety-phenotype with evidence for dysregulation of 5-HT neuronal activity. *Neuropsychopharmacology : official publication of the American College of Neuropsychopharmacology* 40: 1471-1484.
44. Perusini, J. N., E. M. Meyer, V. A. Long, V. Rau, N. Nocera, J. Avershal, J. Maksymetz, I. Spigelman, and M. S. Fanselow. 2015. Induction and Expression of Fear Sensitization Caused by Acute Traumatic Stress. *Neuropsychopharmacology : official publication of the American College of Neuropsychopharmacology*.
45. White, S. L., P. I. Ortinski, S. H. Friedman, L. Zhang, R. L. Neve, R. G. Kalb, H. D. Schmidt, and R. C. Pierce. 2015. A Critical Role for the GluA1

Accessory Protein, SAP97, in Cocaine Seeking.

Neuropsychopharmacology : official publication of the American College of Neuropsychopharmacology.

46. Koutsokera, M., P. Kafkalias, P. Giompres, E. D. Kouvelas, and A. Mitsacos. 2014. Expression and phosphorylation of glutamate receptor subunits and CaMKII in a mouse model of Parkinsonism. *Brain research* 1549: 22-31.
47. Milstein, A. D., W. Zhou, S. Karimzadegan, D. S. Bredt, and R. A. Nicoll. 2007. TARP subtypes differentially and dose-dependently control synaptic AMPA receptor gating. *Neuron* 55: 905-918.
48. Cho, C. H., F. St-Gelais, W. Zhang, S. Tomita, and J. R. Howe. 2007. Two families of TARP isoforms that have distinct effects on the kinetic properties of AMPA receptors and synaptic currents. *Neuron* 55: 890-904.
49. Shi, Y., W. Lu, A. D. Milstein, and R. A. Nicoll. 2009. The stoichiometry of AMPA receptors and TARPs varies by neuronal cell type. *Neuron* 62: 633-640.
50. Kristensen, A. S., M. A. Jenkins, T. G. Banke, A. Schousboe, Y. Makino, R. C. Johnson, R. Huganir, and S. F. Traynelis. 2011. Mechanism of Ca²⁺/calmodulin-dependent kinase II regulation of AMPA receptor gating. *Nat Neurosci* 14: 727-735.
51. Venyaminov SYu, and N. N. Kalnin. 1990. Quantitative IR spectrophotometry of peptide compounds in water (H₂O) solutions. II.

- Amide absorption bands of polypeptides and fibrous proteins in alpha-, beta-, and random coil conformations. *Biopolymers* 30: 1259-1271.
52. Kalnin, N. N., I. A. Baikalov, and Venyaminov SYu. 1990. Quantitative IR spectrophotometry of peptide compounds in water (H₂O) solutions. III. Estimation of the protein secondary structure. *Biopolymers* 30: 1273-1280.
53. Venyaminov, S., and N. N. Kalnin. 1990. Quantitative IR spectrophotometry of peptide compounds in water (H₂O) solutions. I. Spectral parameters of amino acid residue absorption bands. *Biopolymers* 30: 1243-1257.
54. Dong, A., B. Caughey, W. S. Caughey, K. S. Bhat, and J. E. Coe. 1992. Secondary structure of the pentraxin female protein in water determined by infrared spectroscopy: effects of calcium and phosphorylcholine. *Biochemistry* 31: 9364-9370.
55. Dong, A. C., P. Huang, and W. S. Caughey. 1992. Redox-dependent changes in beta-extended chain and turn structures of cytochrome c in water solution determined by second derivative amide I infrared spectra. *Biochemistry* 31: 182-189.
56. Du, M., A. Rambhadran, and V. Jayaraman. 2009. Vibrational spectroscopic investigation of the ligand binding domain of kainate receptors. *Protein Sci* 18: 1585-1591.
57. Mankiewicz, K. A., A. Rambhadran, M. Du, G. Ramanoudjame, and V. Jayaraman. 2007. Role of the chemical interactions of the agonist in

- controlling alpha-amino-3-hydroxy-5-methyl-4-isoxazolepropionic acid receptor activation. *Biochemistry* 46: 1343-1349.
58. Mankiewicz, K. A., A. Rambhadran, L. Wathen, and V. Jayaraman. 2008. Chemical interplay in the mechanism of partial agonist activation in alpha-amino-3-hydroxy-5-methyl-4-isoxazolepropionic acid receptors. *Biochemistry* 47: 398-404.
59. Fabian, H., C. Schultz, D. Naumann, O. Landt, U. Hahn, and W. Saenger. 1993. Secondary structure and temperature-induced unfolding and refolding of ribonuclease T1 in aqueous solution. A Fourier transform infrared spectroscopic study. *J Mol Biol* 232: 967-981.
60. Susi, H., and D. M. Byler. 1986. Resolution-enhanced Fourier transform infrared spectroscopy of enzymes. *Methods Enzymol* 130: 290-311.
61. Schulz, H., B. Schrader, R. Quilitzsch, S. Pfeffer, and H. Krüger. 2003. Rapid classification of basil chemotypes by various vibrational spectroscopy methods. *J Agric Food Chem* 51: 2475-2481.
62. Villarreal-Ramirez, E., D. Eliezer, R. Garduño-Juarez, A. Gericke, J. M. Perez-Aguilar, and A. Boskey. 2017. Phosphorylation regulates the secondary structure and function of dentin phosphoprotein peptides. *Bone* 95: 65-75.
63. Stryer, L., and R. P. Haugland. 1967. Energy transfer: a spectroscopic ruler. *Proc Natl Acad Sci U S A* 58: 719-726.
64. Stryer, L. 1978. Fluorescence energy transfer as a spectroscopic ruler. *Annu Rev Biochem* 47: 819-846.

65. Dolino, D. M., S. S. Ramaswamy, and V. Jayaraman. 2014. Luminescence resonance energy transfer to study conformational changes in membrane proteins expressed in mammalian cells. *J Vis Exp*: 51895.
66. Selvin, P. R., and J. E. Hearst. 1994. Luminescence energy transfer using a terbium chelate: improvements on fluorescence energy transfer. *Proc Natl Acad Sci U S A* 91: 10024-10028.
67. Nir, E., X. Michalet, K. M. Hamadani, T. A. Laurence, D. Neuhauser, Y. Kovchegov, and S. Weiss. 2006. Shot-noise limited single-molecule FRET histograms: comparison between theory and experiments. *J Phys Chem B* 110: 22103-22124.
68. Dolino, D. M., S. Rezaei Adariani, S. A. Shaikh, V. Jayaraman, and H. Sanabria. 2016. Conformational Selection and Submillisecond Dynamics of the Ligand-binding Domain of the N-Methyl-d-aspartate Receptor. *J Biol Chem* 291: 16175-16185.
69. Sisamakakis, E., A. Valeri, S. Kalinin, P. J. Rothwell, and C. A. Seidel. 2010. Accurate single-molecule FRET studies using multiparameter fluorescence detection. *Methods Enzymol* 475: 455-514.
70. Cai, C., S. K. Coleman, K. Niemi, and K. Keinänen. 2002. Selective binding of synapse-associated protein 97 to GluR-A alpha-amino-5-hydroxy-3-methyl-4-isoxazole propionate receptor subunit is determined by a novel sequence motif. *J Biol Chem* 277: 31484-31490.

71. Inanobe, A., H. Furukawa, and E. Gouaux. 2005. Mechanism of partial agonist action at the NR1 subunit of NMDA receptors. *Neuron* 47: 71-84.
72. Stricker, N. L., and R. L. Huganir. 2003. The PDZ domains of mLin-10 regulate its trans-Golgi network targeting and the surface expression of AMPA receptors. *Neuropharmacology* 45: 837-848.
73. Sickmeier, M., J. A. Hamilton, T. LeGall, V. Vacic, M. S. Cortese, A. Tantos, B. Szabo, P. Tompa, J. Chen, V. N. Uversky, Z. Obradovic, and A. K. Dunker. 2007. DisProt: the Database of Disordered Proteins. *Nucleic Acids Res* 35: D786-793.
74. Kumar, S., and M. Bansal. 1996. Structural and sequence characteristics of long alpha helices in globular proteins. *Biophys J* 71: 1574-1586.
75. Jenkins, M. A., G. Wells, J. Bachman, J. P. Snyder, A. Jenkins, R. L. Huganir, R. E. Oswald, and S. F. Traynelis. Regulation of GluA1 $\hat{\pm}$ -Amino-3-Hydroxy-5-Methyl-4-Isoxazolepropionic Acid Receptor Function by Protein Kinase C at Serine-818 and Threonine-840. 618-629.
76. Cheng, Q., S. Thiran, D. Yernool, E. Gouaux, and V. Jayaraman. 2002. A vibrational spectroscopic investigation of interactions of agonists with GluR0, a prokaryotic glutamate receptor. *Biochemistry* 41: 1602-1608.
77. Cheng, Q., and V. Jayaraman. 2004. Chemistry and conformation of the ligand-binding domain of GluR2 subtype of glutamate receptors. *J Biol Chem* 279: 26346-26350.
78. Jayaraman, V. 2004. Spectroscopic and kinetic methods for ligand-protein interactions of glutamate receptor. *Methods Enzymol* 380: 170-187.

79. Cooper, D., H. Uhm, L. J. Tauzin, N. Poddar, and C. F. Landes. Photobleaching Lifetimes of Cyanine Fluorophores Used for Single-Molecule Förster Resonance Energy Transfer in the Presence of Various Photoprotection Systems. *ChemBioChem* 14: 1075-1080.
80. Nick Taylor, J., Q. Darugar, K. Kourentzi, R. C. Willson, and C. F. Landes. 2008. Dynamics of an anti-VEGF DNA aptamer: A single-molecule study. *Biochemical and Biophysical Research Communications* 373: 213-218.
81. Darugar, Q., H. Kim, R. J. Gorelick, and C. Landes. 2008. Human T-cell lymphotropic virus type 1 nucleocapsid protein-induced structural changes in transactivation response DNA hairpin measured by single-molecule fluorescence resonance energy transfer. *J Virol* 82: 12164-12171.
82. Taylor, J. N., D. E. Makarov, and C. F. Landes. 2010. Denoising single-molecule FRET trajectories with wavelets and Bayesian inference. *Biophys J* 98: 164-173.
83. Landes, C. F., A. Rambhadran, J. N. Taylor, F. Salatan, and V. Jayaraman. 2011. Structural landscape of isolated agonist-binding domains from single AMPA receptors. *Nat Chem Biol* 7: 168-173.
84. Levinson, N. M., S. D. Fried, and S. G. Boxer. 2012. Solvent-induced infrared frequency shifts in aromatic nitriles are quantitatively described by the vibrational Stark effect. *J Phys Chem B* 116: 10470-10476.
85. Jenkins, M. A., G. Wells, J. Bachman, J. P. Snyder, A. Jenkins, R. L. Haganir, R. E. Oswald, and S. F. Traynelis. 2014. Regulation of GluA1 α -amino-3-hydroxy-5-methyl-4-isoxazolepropionic acid receptor function by

- protein kinase C at serine-818 and threonine-840. *Mol Pharmacol* 85: 618-629.
86. Yeung, T., G. E. Gilbert, J. Shi, J. Silviu, A. Kapus, and S. Grinstein. 2008. Membrane phosphatidylserine regulates surface charge and protein localization. *Science* 319: 210-213.
 87. Robert, A., and J. R. Howe. 2003. How AMPA receptor desensitization depends on receptor occupancy. *J Neurosci* 23: 847-858.
 88. Milesu, L. S., and C. Nicolai, Bannen, J. 2013. QuB Software.
 89. Qin, F. 2004. Restoration of single-channel currents using the segmental k-means method based on hidden Markov modeling. *Biophys J* 86: 1488-1501.
 90. Zhang, W., S. P. Devi, S. Tomita, and J. R. Howe. 2014. Auxiliary proteins promote modal gating of AMPA- and kainate-type glutamate receptors. *Eur J Neurosci* 39: 1138-1147.
 91. Qin, F., A. Auerbach, and F. Sachs. 2000. A direct optimization approach to hidden Markov modeling for single channel kinetics. *Biophys J* 79: 1915-1927.
 92. Qin, F., A. Auerbach, and F. Sachs. 2000. Hidden Markov modeling for single channel kinetics with filtering and correlated noise. *Biophys J* 79: 1928-1944.
 93. Sumioka, A., D. Yan, and S. Tomita. 2010. TARP phosphorylation regulates synaptic AMPA receptors through lipid bilayers. *Neuron* 66: 755-767.

94. Tomita, S., H. Adesnik, M. Sekiguchi, W. Zhang, K. Wada, J. R. Howe, R. A. Nicoll, and D. S. Bredt. 2005. Stargazin modulates AMPA receptor gating and trafficking by distinct domains. *Nature* 435: 1052-1058.
95. Turetsky, D., E. Garringer, and D. K. Patneau. 2005. Stargazin modulates native AMPA receptor functional properties by two distinct mechanisms. *J Neurosci* 25: 7438-7448.
96. Soto, D., I. D. Coombs, L. Kelly, M. Farrant, and S. G. Cull-Candy. 2007. Stargazin attenuates intracellular polyamine block of calcium-permeable AMPA receptors. *Nat Neurosci* 10: 1260-1267.
97. Jackson, A. C., A. D. Milstein, D. Soto, M. Farrant, S. G. Cull-Candy, and R. A. Nicoll. 2011. Probing TARP modulation of AMPA receptor conductance with polyamine toxins. *J Neurosci* 31: 7511-7520.
98. Rosenmund, C., Y. Stern-Bach, and C. F. Stevens. 1998. The tetrameric structure of a glutamate receptor channel. *Science* 280: 1596-1599.
99. Smith, T. C., and J. R. Howe. 2000. Concentration-dependent substate behavior of native AMPA receptors. *Nat Neurosci* 3: 992-997.
100. Wo, Z. G., and R. E. Oswald. 1994. Transmembrane topology of two kainate receptor subunits revealed by N-glycosylation. *Proc Natl Acad Sci U S A* 91: 7154-7158.
101. Hollmann, M., C. Maron, and S. Heinemann. 1994. N-glycosylation site tagging suggests a three transmembrane domain topology for the glutamate receptor GluR1. *Neuron* 13: 1331-1343.

102. Kuner, T., L. P. Wollmuth, A. Karlin, P. H. Seeburg, and B. Sakmann. 1996. Structure of the NMDA receptor channel M2 segment inferred from the accessibility of substituted cysteines. *Neuron* 17: 343-352.
103. Santos, J. S., G. A. Asmar-Rovira, G. W. Han, W. Liu, R. Syeda, V. Cherezov, K. A. Baker, R. C. Stevens, and M. Montal. 2012. Crystal structure of a voltage-gated K⁺ channel pore module in a closed state in lipid membranes. *J Biol Chem* 287: 43063-43070.
104. Yuan, P., M. D. Leonetti, Y. Hsiung, and R. MacKinnon. 2011. Open structure of the Ca²⁺ gating ring in the high-conductance Ca²⁺-activated K⁺ channel. *Nature* 481: 94-97.
105. Hoffmann, J., A. Gorodetskaia, and M. Hollmann. 2006. Ion pore properties of ionotropic glutamate receptors are modulated by a transplanted potassium channel selectivity filter. *Mol Cell Neurosci* 33: 335-343.
106. van der Cruysen, E. A., D. Nand, M. Weingarth, A. Prokofyev, S. Hornig, A. A. Cukkemane, A. M. Bonvin, S. Becker, R. E. Hulse, E. Perozo, O. Pongs, and M. Baldus. 2013. Importance of lipid-pore loop interface for potassium channel structure and function. *Proc Natl Acad Sci U S A* 110: 13008-13013.
107. Tyutyaev, P., and S. Grissmer. 2017. Observation of σ -pore currents in mutant hKv1.2_V370C potassium channels. *PLoS One* 12: e0176078.

Vita

Caitlin Edmunds Nurik was born in Midland, MI on December 2, 1989, the daughter of Renda Ramsey Edmunds and Mark Lafe Edmunds. After completing her work at Southlake Carroll Senior High School in 2008, she entered Scripps College in Claremont, CA. She received the degree of Bachelor of Arts with a major in biochemistry with honors from Scripps in May, 2013. In August of 2013 she entered The University of Texas MD Anderson Cancer Center UTHHealth Graduate School of Biomedical Sciences.

Permanent address:

1 Hermann Museum Circle Drive
Apt 3047
Houston, TX, 77004